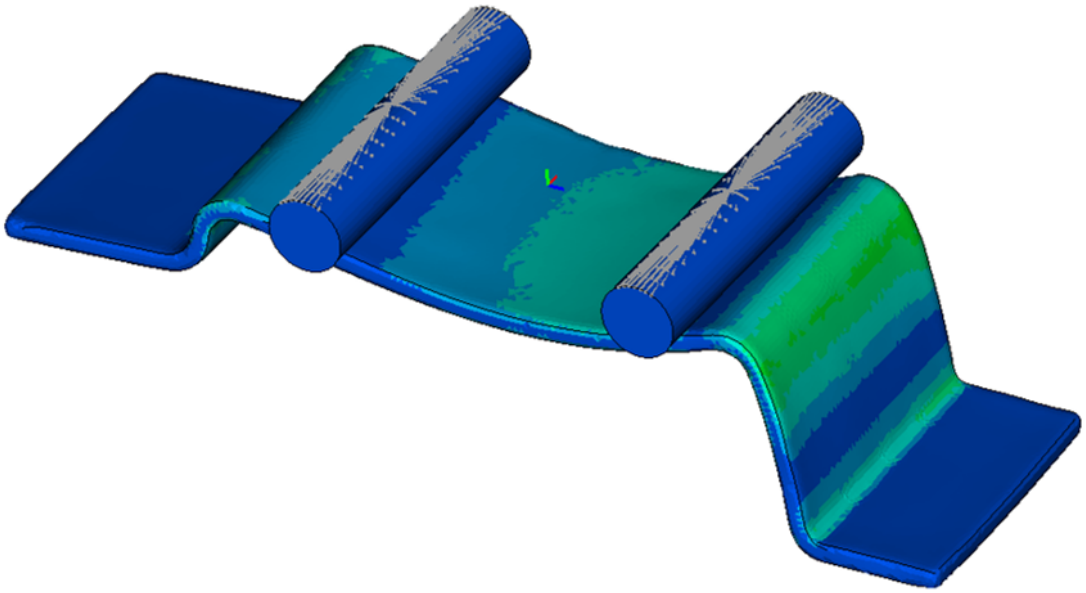

Test Data Input to FE Material Model for SMC

Master's thesis in Materials Engineering

Elin Nilsson

DEPARTMENT OF MECHANICS AND MARITIME SCIENCES

CHALMERS UNIVERSITY OF TECHNOLOGY
Gothenburg, Sweden 2024
www.chalmers.se

Master's Thesis in Materials Engineering

Test Data Input to FE Material Model for SMC

ELIN NILSSON

CHALMERS

Department of Mechanics and Maritime Sciences
Chalmers University of Technology
Gothenburg, Sweden 2024

Test Data Input to FE Material Model for SMC
ELIN NILSSON

Supervisor: Robin Kristiansson, AFRY, CAE & Safety
Supervisor: Mikael Hanneberg, AFRY, CAE & Safety
Examiner: Jim Brouzoulis, Mechanics & Maritime Sciences

Master's Thesis 2024
Department of Mechanics and Maritime Sciences
Chalmers University of Technology
SE-412 96 Gothenburg
Sweden
Telephone +46 31 772 1000

Cover: Finite element model of SMC test object and load applicators, simulated in OptiStruct and visualised in META.

Typeset in LaTeX
Gothenburg, Sweden 2024

Test Data Input to FE Material Model for SMC
ELIN NILSSON
Department of Mechanics and Maritime Sciences
Chalmers University of Technology

Abstract

This thesis aims at correlating Carbon Fiber Sheet Moulding Compound (CF-SMC) composite material tests to a Finite Element (FE) material model. Six different geometrical objects, in total 28 samples, were cut out from two chassis components and they were all three dimensional (3D) scanned to obtain a representative computer aided design (CAD) model. Moreover, they were thermography scanned to detect possible defects or cracks within the material. Destructive testing was done on the samples and a Digital Image Correlation (DIC) setup was used to record the surface strain of the components. With the 3D scanned CAD model of the objects FE models were set up to represent the test. The models was made in detail to capture the test in whole. Multiple problems were found in the test setups which had to be adjusted in order to obtain data possible to compare. Large differences were experienced between the physical tests and FE models which indicated something was not captured correctly in the model or test. Validation tests were done on the machine, clamping systems and load application. Further, a test was done on a stainless steel bracket due to SMC's complexity in material properties makes it difficult to model. Not all tests were performed in the timeframe of the thesis and 13 tests, four objects, were tested. A full correlation were not achieved due to the problems in the test setups. A conclusion is that something in the FE model or tests, is not behaving as expected and more eliminations is needed to eliminate errors to reach a good correlation.

Keywords: Short fiber composite, SMC, material testing, destructive testing, non-destructive testing, FE material model, correlation.

Preface

This report presents the outcome of a master's thesis project done at the CAE & Safety group at AFRY Trollhättan, with collaboration with a U.S. based vehicle developer. Further, it was carried out at the Department of Mechanics & Maritime Sciences at Chalmers University of Technology during the spring of 2024.

Acknowledgements

The writer would like to thanks the examiner Professor Jim Brouzoulis for the support and guidance. Further, a big thank you to the supervisors Robin Kristiansson and Mikael Hanneberg for the constant support and feedback throughout the thesis. Lastly, a thank you to the co-workers at AFRY for the feedback and the enjoyable working environment.

Elin Nilsson, Gothenburg, June 2024

List of Acronyms

Below is the list of acronyms that have been used throughout this thesis listed in alphabetical order:

2D	Two Dimensional
3D	Three Dimensional
CAD	Computer Aided Design
CHEXA	Hexagonal Solid Elements in OptiStruct
CQUAD4	Quadratic Shell Elements in OptiStruct
CT	Computational Thermography
CTETRA	Tetrahedral Solid Elements in OptiStruct
CTRIA6	Second Order Triangular Shell Elements in OptiStruct
DIC	Digital Image Correlation
MROM	Modified Rule of Mixture
ROM	Rule of Mixture
RBE2	Rigid Body Element 2
RBE3	Rigid Body Element 3
SMC	Sheet Moulding Compound
SPC	Single Body Constraint
UTM	Universal Testing Machine

Nomenclature

Below is the nomenclature of indices and parameters that have been used throughout this thesis.

Indices

x,y,z	Index for local direction
X,Y,Z	Index for global direction

Parameters

a_1	Change in observation angle
a_2	Change in observation angle
a_3	Change in observation angle
a_4	Change in observation angle
a_5	Change in observation angle
a_6	Change in observation angle
a_7	Change in observation angle
a_8	Change in observation angle
χ_1	Orientation factor
χ_2	Effective length of fibers
χ_3	Orientation factor
χ_4	Effective length of fibers
$\Delta\sigma$	Variation in first stress variant
ΔT	Change in temperature
E_c	Young's modulus for composite
E_f	Young's modulus for fibers
E_m	Young's modulus for matrix
K_0	Thermoplastic constant

σ_{cu}	Ultimate strength of composite
σ_{fu}	Ultimate strength of fibers
σ_{mu}	Ultimate strength of matrix
T_0	Average temperature
V_c	Volume fraction of fibers
r_0	Radiometric transformation, original state
r_1	Radiometric transformation, transformed state
X_{error}	Error in displacement
X_{SMC}	Displacement recorded on SMC
X_{steel}	Displacement recorded on steel
x_t	Transformed location in x
y_t	Transformed location in y

Contents

List of Figures

List of Tables

1
Introduction

In automotive industry the usage of composite material has increased over the last decades [1]. Some of the main benefits of using composites materials are for their high stiffness to weight ratio which enables the possibility for weight reduction of the components while keeping their structural integrity. Further, they also have desirable corrosion resistance and a high flexibility in design possibilities due to the manufacturing methods. Some drawbacks of composites are the costs, they are typically a quite expensive material to purchase and expensive to manufacture. Another drawback is their complexity in strength and stiffness due to their dependence of the fibers direction in the matrix [2].

Sheet moulding compounds (SMC) is a process to manufacture a short fiber composite material where the fibers are randomly distributed. It is widely used in the automotive industry due to it being relatively low cost composite. However, due to the materials short fibers and random fiber orientation the fiber content can vary across a component which then results in stiffness and strength parameters also varying over the part [3]. To make accurate finite element (FE) models of these components can be difficult. The material model used by AFRY does not take the varying properties of the material into account. Due to the parts being moulded using compression moulding some geometrical features can compromise the performance of the component. This is due to the way the matrix and fibers flow during the moulding process which can result in fibers aligning or not keeping the fiber content constant over the component [4]. Some problematic features such as radii, ribs and tight corners are suspected to affect the properties a great deal which is due to the challenging manufacturing method and flow pattern during moulding. To create an accurate FE model and understanding of the material is necessary and in this thesis data from material tests will be analysed, compared and correlated to the currently used material model. The physical tests that will be performed are thermography scans and digital image correlation (DIC) where strain data will be recovered and destructive tests where samples are loaded until failure which is done on cut-outs from the investigated sections.

1.1 Aim

The thesis aims to analyse a component's stiffness and strength where radii and ribs are present through physical tests. Further, to investigate its importance in an FE model and correlate the material behaviour from the tests to the FE model as well as investigating possible methods on how to model the material.

1.2 Objective

SMC material will be studied by performing material test on six different samples with varying geometry, they contain geometrical features that have been identified as critical. By analysing the data from tests, FE models will be set up to be able to predict the material behaviour in these components. The FE model will be correlated to the material tests in order to make it possible to use it for other components with the same material and similar critical features.

1.3 Limitations

In this thesis there is a limit on what material properties will be investigated through the material tests and FE model. The fatigue behaviour of the SMC will not be investigated. Further, environmental influence on the material, such as temperature and humidity sensitivity, will not be investigated. Moreover, the flow behaviour of the SMC when moulding will not be investigated, however the consequences in the terms of fiber volume fraction and fiber orientation will be considered. During the timeframe of the thesis not all samples will be possible to test and the tests will be limited to three out of six possible objects. Not all samples will be modeled in detail throughout the project.

2
Theory

In the following chapter theory is presented from a literature study regarding the areas which are relevant for the thesis. Material properties, manufacturing methods and the test methods are presented further in this chapter.

2.1 Sheet Moulding Compound

SMC is a composite material widely used in automotive industry due to having appropriate mechanical properties, low weight and being a relatively cheap composite [3]. SMC is a short fiber composite in which the fibers have a random orientation and distribution. The material is typically made as a pre-impregnated sheet which needs further forming processes to mould and cure into a finished product. Compression moulding is a manufacturing technique which can be used to form the material into desired components which gives possibilities in designing complex geometries [5]. Moreover, the material structure is made up of chips or bundles where the fiber locally go in the same direction although globally the material has randomly order fibers or chips. See Figure 2.1 for a schematic showing the chips in an SMC where one chip is marked with red outline.

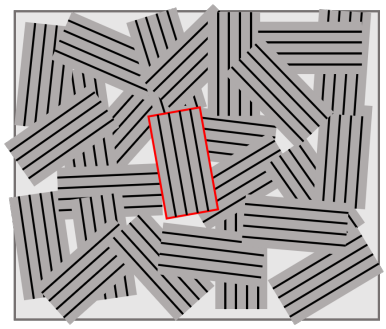

Figure 2.1: Schematic of SMC structure where the chips are shown as gray squares with black lines representing fibers. One chip is marked with a red outline.

For a composite material its constituents play an important role. The fibers are what gives the material its strength and stiffness while the matrix material is there to protect and help with load transfer to the fibers. In most cases the matrix is less structural than the fibers [6]. It is common that composites are composed of long fibers and a matrix, commonly a thermoset polymer. When composites are fabricated this way they typically have highly anisotropic behaviours due to the fibers not being oriented equally in all directions [7]. For SMC this is not the case, due to its random orientation of short fibers it is a quasi isotropic material. This is generally a good approximation on how the material behaves, for SMC FE models however in certain cases due to challenging geometry such

as ribs and small radii, and manufacturing defects the SMC can not always be assumed to be quasi isotropic [8]. This can also be due to a complex flow pattern during the compression moulding which can result in varying fiber content and fiber orientation [4]. One example of this is when two sheets are moulded together, this can result in a seam between the fibers where they align along the edge, a so called weld line which is described in Chapter 2.1.2.2. This can be one reason for defects in the material which can reduce its performance [8].

The components of SMC materials can vary heavily and it is commonly made out of some kind of synthetic fiber reinforcement such as glass or carbon fibers and a polymer matrix such as polyester, vinylester and epoxy [2]. Since the matrix is often a thermoset polymer it needs to endure some sort of curing process to get it to harden in the wanted position, this can be performed through heating the composite or in room temperature. During the curing the polymer goes through a chemical reaction where the polymer chains start to cross-link which gives the polymer its hard and brittle nature [9].

The material treated in this thesis is a carbon fiber and epoxy SMC (CF-SMC). The material used has the material properties described in Table 2.1. The components are manufactured with a SMC pre-impregnated fibers and compression moulding to form the desired components.

Table 2.1: Material properties of the relevant CF-SMC [10].

Property	SMC
Density [g/cm^3]	1.46
Fiber Content [%]	53
Fiber Length [mm]	25.4
Glass Transition Temperature [°C]	130
Tensile Strength [MPa]	150
Tensile Modulus [GPa]	33
Flexural Strength [MPa]	330
Flexural Modulus [GPa]	25

2.1.1 Manufacturing Processes

Typically, SMCs are first manufactured as a sheet of the desired materials and composition. This sheet is used in a second step where the material is moulded to a component which then has the desired shape and design. This is can be done through compression moulding where the part also gets cured in the same process. After this there is generally some post processing done to achieve the finished component [11].

2.1.1.1 SMC Manufacturing

SMCs are often made as a prepreg sheet, which is a pre-impregnated composite, and then used for moulding of the material to a component [11]. It contains resin, fiber, fillers and lubricant. A schematic of the SMC prepreg manufacturing process can be seen in Figure 2.2. A carrier film is first covered with pre-mixed resin. On top of this a chopper arbor cuts continuous fibers to the desired length, usually between 25-50mm depending on the

material. These fibers then fall down on the carrier film and resin. It is crucial that the fibers have a correct length and equal distribution all over the resin to achieve an evenly distributed fiber and matrix ratio. The fibers' orientation will be stochastic, however to get an even distribution in the epoxy is important to get the desired properties of quasi isotropic behaviour. Further, a top carrier film gets coated with a resin paste and then applied on top of the lower carrier film, resin and fiber mixture. All of this goes through a system of rollers to distribute the resin and wet all fibers. After this the prepreg is rolled to a cylinder. The two carrier films are typically a polymer and they are important to enable the prepreg to be coiled as well as preventing contamination and monomer evaporation of the fiber and resin mixture. After the SMC manufacturing procedure the prepreg is stored for a certain time to achieve the desired viscosity to be able to further use it in manufacturing [12, 13, 5].

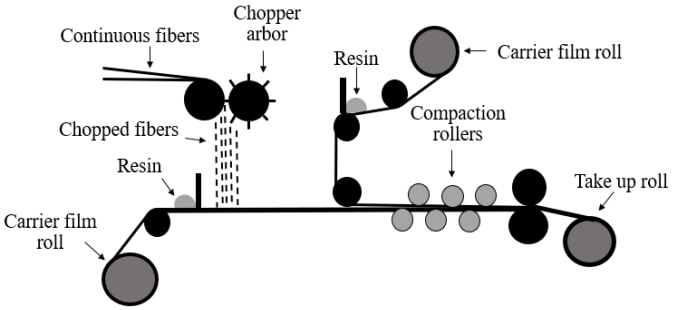

Figure 2.2: Schematic of manufacturing process of SMC prepreg where all parts of a production chain are present. Adapted from [5].

2.1.1.2 Compression Moulding

To manufacture parts using SMC it is often combined with compression moulding. A schematic of this process can be seen in Figure 2.3. The process can be described in the following steps: the desired amount and layers of SMC, so called charge, is placed in the compression mould which is pre-heated. To what temperature is dependent on the material and mould cycle. Then, the top and bottom half closes and the SMC is spread out in the mould. In the next stage the mould is heated to around $120° - 150°$ depending on the material. Following step is to cure the material in the mold which takes around $60 - 120s$. Lastly, the mould opens and the part is ready for further processing if needed [14, 13].

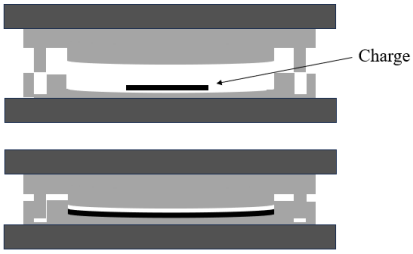

Figure 2.3: Schematic of compression moulding with one open mold where charge is placed, this is the top figure and one closed where the charge has been pressed out, this is the lower figure. Adapted from [13].

2.1.2 Material Behaviour

Due to most SMC being manufactured in similar ways they have some expected properties which are typical for the material. First as mentioned previously, the orientation of the fibers is stochastic hence the material is quasi isotropic.

To evaluate a composite's stiffness and strength it is common to refer to the rule of mixtures (ROM) which is a way to differentiate and determine the longitudinal and transverse properties in continuous fibers, it can be seen in Equation (2.1) [15].

$$E_c = V_f E_f + (1 - V_f) E_m \tag{2.1a}$$
$$\sigma_{cu} = V_f \sigma_{fu} + (1 - V_f) \sigma_{mu} \tag{2.1b}$$

Where E_c is the elastic modulus for the combined composite, E_f and E_m is the elastic modulus for the fiber and matrix respectively, V_f is the volume fraction of the fibers, σ_{cu}, σ_{fu} and σ_{mu} is the ultimate strength for the composite, fiber and matrix.

Since SMC has a stochastic orientation of the short fibers the traditional ROM has to be adjusted accordingly. One way to take the fiber length and fiber orientation into account is through the modified rule of mixtures (MROM), which can be seen in Equation (2.2) [15].

$$E_c = \chi_1 \chi_2 E_f V_f + (1 - V_f) E_m \tag{2.2a}$$
$$\sigma_{cu} = \chi_3 \chi_4 V_f \sigma_{fu} + (1 - V_f) \sigma_{mu} \tag{2.2b}$$

Where the χ_1 and χ_3 are orientation factors and χ_2 and χ_4 the effective length of the fibers. Further, the distribution of the fiber is important for the strength of the material. If the volume fraction is varying over the component, so will the strength and stiffness of the part.

2.1.2.1 Mechanisms in SMC

The failure of SMC can be complex due to multiple constituents and their influence on each other. A typical stress-strain curve can be seen in Figure 2.4 where linear and non-linear regions can be observed. The non-linear region begins when micro-cracks start to form in the matrix, this point is called a knee. The micro-cracks can be seen as crazings on the surface of the test sample. Crazings typically show up as white markings in a polymer during tensile or bending loads, they are most common in glassy and brittle polymers [16]. Even though crazings are present in this stage the material will not break fully hence the material can still carry load which can be seen in Figure 2.4 [17].

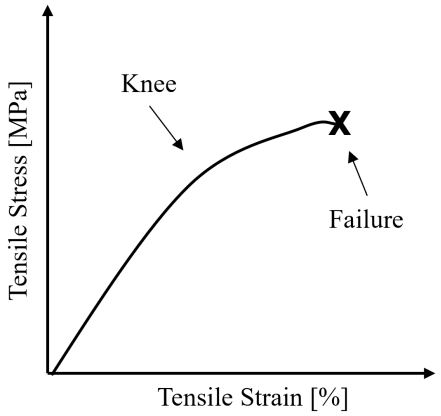

Figure 2.4: Typical stress-strain curve for SMC where the knee and failure is pointed out. Adapted from [18].

The failure modes most often seen in SMC are matrix cracking, interface debonding and fiber pull-out. Fiber breakage is seen less in short fiber composites compared to continuous fibers which is due to the fiber's length. The most common failure however is matrix failure due to it usually being the least structural constituent in the composite [4, 19, 20].

The failure in the material can initiate in different positions in the sample. For composites a common failure mode is interlaminar failure, this is when the crack propagates within the material. An example of this is delamination which is when the layers of the composite separate and a crack propagates between layers. Interlaminar failure is caused by either interlaminar tension, compression or shear loads [21]. Since a randomly oriented SMC has big difference between the chip orientation the effective load transfer between the chips is reduced. Due to this, a SMC with random orientation's weakest area is the interface between the chip and matrix. Further, the randomness of the chips the crack propagation is not continuous but rather has a stopping motion during the failure due to the fiber load transfer [22].

2.1.2.2 Weld lines

When using SMCs during compression moulding one issue that can compromise the properties of the material is weld lines. This is when two or more flows meet during compression moulding. This can cause a change in the orientation of the fibers along the weld line due to the fibers aligning with the flow instead of mixing together, this creates a region with low fiber content. Further, it can cause v-notches due to uneven cooling which will result in stress concentrations and can result in premature failures. It can also cause air traps and pores which have similar effects. In the weld lines there is also a risk of poor entanglement of the polymer molecules which results in a weaker spot of the polymer. All of these effects may result in a change in stiffness and strength for the material locally [23].

2.2 Tests

Three different test methods are used to analyze the SMCs' behaviour and their theory is described in the following sections. Thermographgy scans are described in Chapter 2.2.1, it is a non-destructive testing method where the material is investigated for the presence of external and internal cracks and voids while keeping the testing sample intact. Digital image correlation (DIC) is described in Chapter 2.2.2 and it is a method where strain data can be extracted from the surface on a sample during a test. Lastly a constituent test is described in Chapter 2.2.3 which is a method to define the volume fraction of each of the constituents, fibers and matrix.

2.2.1 Thermography

Scanning a material with thermography is a way to look for pores, voids and cracks externally and internally. It is a technique where the temperature of a component is analysed through infrared rays detection using a thermal-camera. A two dimensional (2D) temperature field is mapped. When deviations are found in the materials temperature due to different thermal properties, it can mean the presence of a crack or void in the material [24, 25].

Infrared thermography can be used passive and active which refers to how the heat source is applied to the investigated object. For the passive infrared thermography the test sample has a different temperature to the environment which results in the camera being able to capture the temperature field. In an active infrared thermography however the heat is coming from an external light and heat source. The thermoelastic effect can be assumed, which is a reversible temperature variation that occurs in a solid due to volume variation. In Equation (2.3) an experimental expression for thermoelasticity is described.[24, 26, 27].

$$\frac{\Delta T}{T_0} = -K_0 \Delta \sigma \tag{2.3}$$

ΔT is the change in temperature, T_0 is the average temperature of the solid, K_0 is the thermoelastic constant and $\Delta\sigma$ is the variation in the first stress variant.

In the case of anisotropic materials the same equation can be assumed to hold however it will be dependent on what direction is studied due to the anisotropic properties in the material.

When a temperature profile is obtained from a thermograpgy scan a typical graph from an area without any defects can be seen as the blue point 1 line in Figure 2.5. If the plot is observed the orange point 2 curve is deviating from the blue curve which indicated a defects such as a void, porous region or a crack.

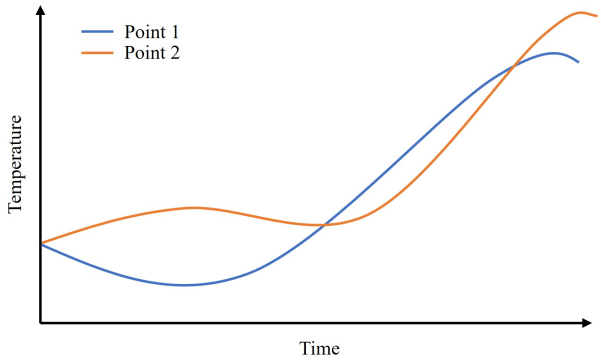

Figure 2.5: Typical temperature profile with a non-defective line (blue, point 1) and a defective line (orange, point 2). The defective line does not follow the expected blue line which indicated a defect.

2.2.2 Digital Image Correlation

DIC is a way to measure deformation on the surface of a component with the help of cameras to record the displacement of the surface. From this strain and deformation data can be extracted. The technique is used in material tests in a similar way an extensometer can be used when doing a tensile test. The surface of the inspected component is colored with paint which have dots randomly placed, a speckle pattern, which gives gray value information which further can be evaluated in the camera images [28, 29, 30]. See Figure 2.6 for an example on how the speckle pattern can look.

Figure 2.6: A typical speckle pattern painted on a surface prepared for DIC [29].

To be able to measure and evaluate three dimensional (3D) coordinates and displacements a stereo camera setup is necessary. This way, triangulation between the two cameras can be used in order to locate the deflection on the component in a 3D space. To be able to get an accurate result the calibration of the camera and test sample setup is important. The camera parameters can be divided into two groups: intrinsic and extrinsic. The intrinsic parameters are dependant on the camera model used. It is important to know the lens distortion and aberrations of the camera model to have an accurate test. Ideally, the values are exactly known and can be included in the mathematical model to compensate to have an accurate measurement setup. The extrinsic parameters describe the two cameras relative position to each other which is necessary for the triangulation of the coordinates [31].

When having the two camera images, the speckle pattern is divided into smaller squares, so called facets. These facets can be of varying size and distribution on the surface of

the component. The other camera image will identify these squares in a larger scale, see Figure 2.7. When the surface deforms the facets will deform which can be used to calculate the local deformation of the component. The facets from original state to deformed state can be seen in Figure 2.7 [31]. In this thesis the GOM Aramis system us used which is a DIC system provided by Zeiss.

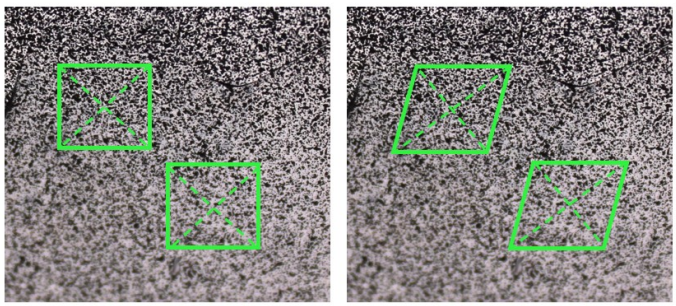

Figure 2.7: Before and after surface deformation where the facets, portrayed as green squares, has deformed. Adapted from [31].

2.2.2.1 Deformation Calculation

For the calculation of the surface strain according to the Zeiss GOM strain mapping system is as follows [31]. To calculate and identify the deforming image there exists many version however the one which will be used in this thesis is described below.

One main assumption is that the original and deformed state of the picture have a causal relationship which can be described with $f(x, y)$ and $g(x_t, y_t)$ where $f(x, y)$ is the original state's coordinates and $g(x_t, y_t)$ is the deformed state's coordinates. A correlation between the original and deformed state can be described as in Equation (2.4) where Δx and Δy are directional displacements in x and y.

$$c(\Delta x, \Delta y) = \frac{f(x, y), g(x + \Delta x, y + \Delta y)}{|f(x, y)| \cdot |g(x, y)|} \tag{2.4}$$

With this, two different subsets of pixels, which represents facets and search area, can be defined at two different locations. To know the maximum similarity between these subsets a subpixel interpolation can be done, usually bilinear, bicubic or spline interpolations are used. Using this as an iterative algorithm the gray value of the squares can be minimized, to maximize the data output.

Assuming that the observation angle changing will lead to changes in the perspective of the image. To define the scanned positions a pseudo affine transformation can be used, this can be seen in Equation (2.5).

$$\begin{aligned} x_t &= a_1 + a_2 x + a_3 y + a_4 xy \\ y_t &= a_5 + a_6 x + a_7 y + a_8 xy \end{aligned} \tag{2.5}$$

Where a_1, a_2, a_3, a_4, a_5, a_6, a_7 and a_8 are the change in observation angle dependent on x,y and x_t is the transformed x parameter and y_t is the transformed y parameter.

To transform the original state to a deformed state radiometric transformation [31] can be used, this considers the changes in how much the surface is illuminated as well as the perspective distortions. It can be seen in Equation 2.6.

$$f(x, y) = r_0 + r_1 \cdot g(x_t, y_y) \tag{2.6}$$

Using this model, matching the original and deformed pictures is done by an overdetermined system of equations where the gray value gradients give more information as well as describing the change in the gray value distribution. Because of this more values are needed to determine the gray value differences and further to minimise the deviation in (2.6). A way to solve this is with Newton-Raphson method. In Equation 2.7 this can be seen.

$$min \sum_{i=1}^{n} |f(x_i, y_i) - (r_0 + r_1 \cdot g(x_t, y_t))|^2 \tag{2.7}$$

To be able to determine the z value of the 3D coordinates triangulation between two cameras is necessary. This is done by correlating the middle point of each facet in the two cameras. These points are then used during a triangulation to transfer from 2D to 3D.

To evaluate the strain data from the DIC can be done through plotting the local deformation all over the sample. This is then used to map the strain over the entire sample, in Figure 2.8 this can be seen.

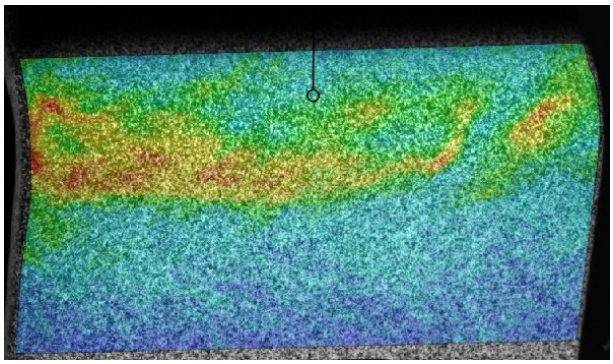

Figure 2.8: Picture showing how the strain mapping can look over a surface where red indicated higher strain and blue lower strain on the surface.

2.2.3 Constituent Content Testing

One way to analyse the volume fraction of fiber and matrix in a composite is through constituent content testing. This can be done by removing the matrix from the fiber and then weighing the fiber content. By doing this the volume fraction of each constituent can be determined. American Society for Testing and Materials (ASTM) have a standard relating to the constituent testing in composite materials were a description of the process is defined [32, 33]

There exists two different methods to remove the matrix. For Method I the matrix is physically removed by ignition, digestion or carbonization. By doing this the fibers should remain unharmed which allows measuring the fraction (weight or volume) of each constituent of the composite, it is also possible to know if there were voids present in the material. Method II can only be used if the laminate's constituents have a known areal weight. It is used to calculate the volume or weight fraction by measuring the thickness of a cured laminate. However, using this method there is no possibility to measure the void content in the laminate [32].

3
Methods

In this chapter the overall test plan as well as the test methods for the tested objects are described. The chapter divided into the overall testing procedure and specific description regarding each object. Both non-destructive and destructive tests were performed.

3.1 Test Objects & Test Plan

Six different objects with different geometries were investigated (see Appendix A for all objects). In Figure 3.1 and Figure 3.2 two examples of objects are presented, here it is object 2 respectively object 4. The samples were cut by hand from chassis components were the number of samples were between one to three samples.

Figure 3.1: Example of sample geometry, here showing the object 2.

Figure 3.2: Example of sample geometry, here showing the object 4.

To minimize the risk of defects within all samples due to being cut from the same component two chassis components were used to cut samples from. The same number of samples were cut from each component and this is refereed to as two batches of samples. In total the number of samples per object varied between two and six and in total 28 samples were cut. A summary of the number of objects, batches and samples can be seen in Table 3.1.

The objects have different shapes to capture the behavior of the material in areas with complex geometries such as small radii or ribs, which was the expected weaker and problematic areas in the components. The objects were selected prior to the start of the thesis.

Table 3.1: Summary of test samples where the number of batches, samples and sample total of each object is summarised.

Object	Batches	Samples	Sample Total
1	2	3	6
2	2	2	4
3	2	2	4
4	2	1	2
5	2	3	6
6	2	3	6
Total			28

A testing plan was developed and a testing order was decided. The motivation behind the order was the complexity of the test samples and which of the test fixtures were finished when testing was planned to start. The order was as followed: object 2, 4, 5, 1, 3, 6. Not all tests were tested within the limited timeframe of the thesis and the objects which were tested were object 2, 4, 5, 1 and the method is described in the respective sections below. The test setups were decided prior to the thesis start however some adjustments were done which is further described in the respective sections. The test machine used for the tests of the samples was a Instron universal testing machine (UTM).

3.2 Overall Test Procedure

The overall testing procedure were similar for the tested samples and the steps concerns all of them are described in this section.

Firstly, all samples were 3D scanned in order to obtain a representative CAD model of each sample. This CAD model has as precise geometries, including possible surface defects, as the sample as possible which was preferable to use for the FE models. After this, the samples where thermography scanned to detect any pores, voids, cracks or other defects within the material prior to testing. Next, the samples were painted with a speckle pattern to be prepared for the GOM system to capture the surface deformation and lastly the destructive test could be performed. During the destructive test to record it four cameras were used: one DSLR camera which recorded the test in high quality, one GoPro camera to see the test in one more angle and two cameras connected to the GOM system. The destructive test setup was varying between the components and the specific setup used for each sample can be seen in the following sections.

3.3 Test Procedure Object 2

The first tested sample was object 2. In total four tests were performed and two test setups were used. The sample was set up in the machine which included putting it correctly in the test fixture and adjusting all cameras which were on during the test.

For object 2 the setup planned for the sample looked according to Figure 3.3. The load applicator was cylindrical with a diameter of 10 mm. To validate if the setup was good two tests were carried out which did not break the sample. The first test was performed to 25% of the predicted critical displacement of the object and the second test was performed to 50% of the predicted critical displacement. When they were acceptable and no faults could be seen a full test until failure of the sample was performed. The tests performed to 25% and 50% of the predicted critical displacement respectively was only carried out on the first tested sample from the object, the remaining samples were tested directly until failure. During the tests the rate which the load was applied was 3.40 mm/min and the frequency the GOM system was recording was 15 Hz for the first two tests which did not break the sample and for the last test until failure the GOM system recording frequency was 5 Hz.

After the test was performed on the first sample some problems were encountered with the test fixtures and clamping method which led to a change needed in the setup. The clamped area was moved higher on the sample in order to avoid a large deflection when loading the sample and in an attempt to force the crack formation to the radius where the GOM cameras were aimed. This new setup is represented in Figure 3.4.

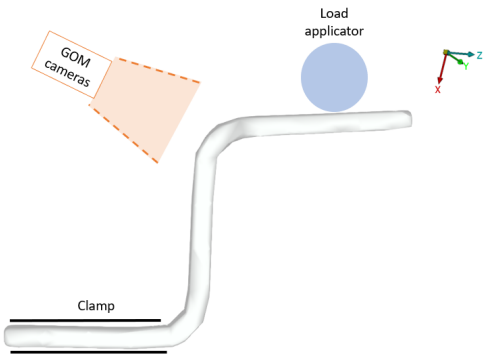

Figure 3.3: Schematic showing the first test setup for object 2. The GOM cameras' placement is represented with a orange schematic, the cylindrical load applicator is represented as a blue circle and the clamp with black lines.

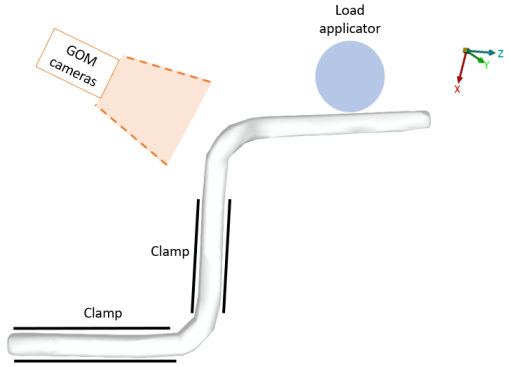

Figure 3.4: Schematic showing the second test setup for object 2. The GOM cameras' placement is represented with a orange schematic, the cylindrical load applicator is represented as a blue circle and the clamp with black lines.

Due to previously mentioned problems with the setup a new thermography scan was done on the first tested sample, after the first test were performed. This was in order to investigate if there was a defect in the material which could have impacted the tested result. After this, a second test was carried out on the same sample with the new setup. Furthermore, the remaining three samples were tested according to the adjusted setup, however no second thermography scan was performed since it was deemed unnecessary.

3.4 Test Procedure Object 4

Object 4 had in total two samples, one per batch. The sample was placed in the test fixture and later all cameras were aimed in the correct placement. Three cameras were used where one was recording the sample and was aimed from the side of the sample and two were connected to the GOM system and aimed to the area of expected crack initiation. During this test the GoPro was not used.

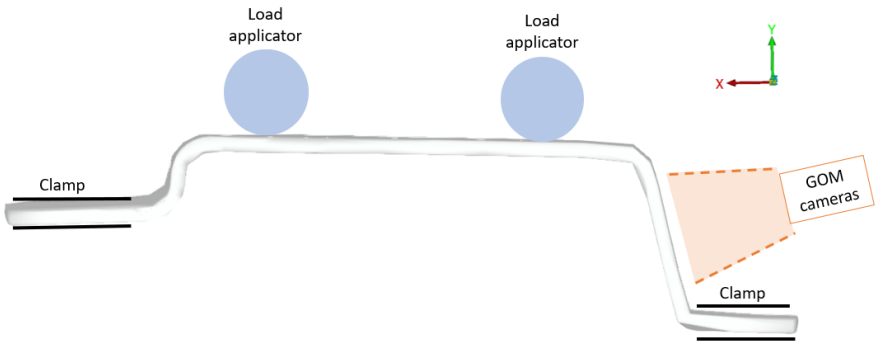

Figure 3.5: Schematic showing the test setup for object 4. The GOM cameras' placement is represented with an orange triangle, the two load cylindrical applicators with blue circles and the clamps with black lines.

This sample had a test setup according to Figure 3.5 where clamped area, load application positions and GOM cameras aim can be seen. The cylinders which applied the load had a diameter of 10 mm. When the first sample of object 4 were set up for testing a test was performed which was stopped after 50% of the predicted critical displacement evaluated prior to testing. This was done to confirm the test setup and to see if any problems such as slipping sample, cameras not capturing the correct area and so forth could be detected. When this was approved a full test was done until failure for the sample and all remaining samples after the first were all tested until failure directly due to already tested setup. The velocity of the load application was 0.60 mm/min and the frequency which the GOM was recording was 5 Hz for the first test where 50% of the predicted critical displacement and for the test until failure the frequency was 1 Hz.

3.5 Test Procedure Object 5

In total there were six samples for object 5, three from each batch. The sample was placed in the test setup which was constructed as shown in Figure 3.6.

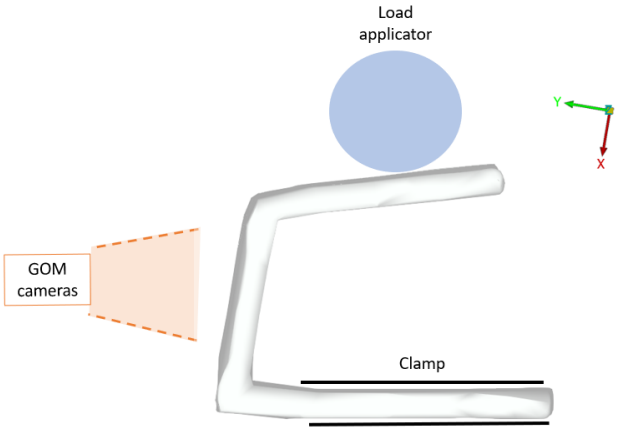

Figure 3.6: Schematic showing the test setup for object 5. The GOM cameras' placement is represented with an orange triangle, the cylindrical load applicator with a blue circle and the clamp with black lines.

In Figure 3.6 the setup is shown and the cylinders have the diameter 25 mm and the measurements on where the clamps were placed can also be seen in Figure 3.6. Similarly to previously tested objects the first sample of object 5 was first tested to 50% of the predicted critical displacement in order to evaluate the setup if anything need to be adjusted. After this all tests were loaded until failure. The velocity of the test was 3 mm/min and the frequency on the GOM recordings were 1 Hz on all tests done on samples of object 5.

3.6 Test Procedure Object 1

Object 1 has in total six samples, however only one samples were tested within the timeline of the thesis. When the test setup were revised prior to test it was found that the original planned way to test the sample where not good with the respect to the visibility of the GOM cameras. Due to this the sample was flipped and the load was applied in the opposite direction which was first planned. Moreover, a more iterative approach was implemented in regards to see if the test setup was satisfactory before testing until failure of the sample. An FE model was setup and compared to the first test without failing in order to capture possible problems in the setup. The non-destructive test had a load limit which was 50% of the predicted critical load, which was 75 N. This result was then compared to the FE model result and a decision could be taken regarding to keep or change the test setup. The setup used for the test can be seen in Figure 3.7.

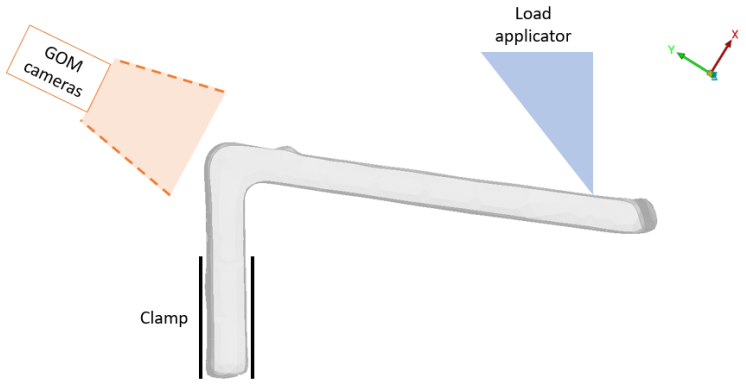

Figure 3.7: Schematic showing the test setup for object 1. The GOM cameras' placement is represented with an orange triangle, the triangular load applicator as a blue triangle and the clamp as black lines.

The adjustments included changing the way the sample was clamped in the fixture. The previous way was problematic due to the sample moving when it was clamped, it rotated inside the clamp. This was solved by changing the bolt position of the clamp. This way the entire area which was intended to be clamped would be. See the different clamping positions in Appendix C. Moreover, the load applicator was changed. This due to clips bending and flexing during the test in the previously used system with a cylinder. The new load applicator was a solid aluminium block with a triangular shape, see Appendix C.

To decide the height of which the sample should be clamped some different measurements were testes in the FE model. A concern was raised during the first test that the sample was clamped rather far down and it could risk the sample breaking just above the clamped area rather than somewhere else in the sample which is preferred. Ideally the clamp is as far away from the expected failure position as possible. However, if the clamped were moved too far upwards similar situation could occur if it was placed too close to the radius. A middle ground was found which can be seen in Figure 3.7.

3.7 Test Procedure Stainless Steel Test

In order to test a simpler material to model and to validate the test method it was decided to test with the same setup as for object 1 with a stainless steel plate. This was done in order to investigate if the model and test setup needed to be adjusted or it could be the sample that had defects which could explain not expected results.

The geometry of the test sample was according Appendix A where the test setup was according to Figure 3.8 and made out of stainless steel. The sample had a thickness of $1,94$ mm. The setup used was the same as described in Chapter 3.6 for the test of object 1. The test was not made in order to break the stainless steel sample but only to test the elastic part in the sample. The test was run until 80 N and then aborted in order to investigate the elastic response only.

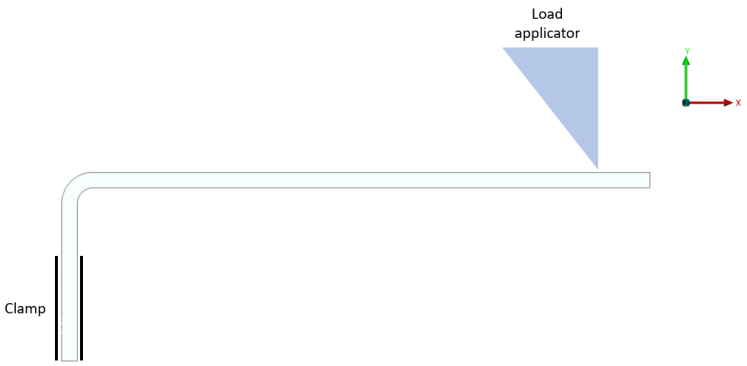

Figure 3.8: Schematic showing the test setup for the stainless steel sample. The triangular load applicator is represented with a blue triangle and the clamp is represented with black lines.

3.8 Validation of Test Equipment

To validate that the displacement the machine registers it accurately a validation test was done. When a tensile test machine is used with time, the crosshead can start to bend. This will further affect test results and not give an accurate measurement of the displacement. To test if this was a problem in the test machine a validation test supported by the manufacturers of the machine was carried out [34].

To begin with, the same load applicator was used which is important since the validation is done depending on test setups. First, a test was done on something considered stiff in order to compare to the SMC. A thick steel plate was used as a rigid test specimen. The test was done until 75 N and the displacement was recorded in the machine. Next, the same test was done on the object 1. The two tests were compared and the error between the two was calculated according to Equation (3.1).

$$X_{error} = X_{SMC} - X_{steel} \tag{3.1}$$

Where X is the deformation recorded for the error, SMC sample and steel respectively.

One more validation test was performed on the object 1 test setup described in Chapter 3.6. A concern with the setup was that the sample would be sliding in the clamped area. To validate if this was a problem the test described in Chapter 3.7, on the stainless steel sample, was performed with two types of clamps. The first test was done with the same clamps used for the original test as well as object 1 test setup. In the second test a wedge clamp was used. In both tests the sample was loaded to 75 N and was clamped to the same measurements on the sample. See the test setups in Appendix C

3.9 Data Handling & Analysis

From the destructive testing multiple data types where obtained: first raw data from the machine where time, force and displacement were logged. This was in a csv-file which is possible to open in Microsoft Excel or other data handling programs. The raw data were handled mostly in Microsoft Excel in the thesis, were force-displacement graphs were made

in order to compare between FE model and tested result. Since all tests were recorded the videos capturing the tests were analysed in order to detect potential problems with the tests. It was useful when the GoPro was introduced which meant the test could be viewed from multiple angles.

From the GOM system a ginspect-file was obtained which is the file format that Zeiss Quality Suite with the added app Zeiss Correlate Pro supports to look at the surface strain data. From this the surface strain could be evaluated in points chosen by the user or an overall average on the surface. In order to compare the tested samples and FE model the surface strain could be mapped from the test and from the FE model.

4
Modeling

The model methods for object 4, 1 and stainless steel sample are described in the following chapter. For all models ANSA (v24.1.0) was used as a preprocessor, Altair OptiStruct (v21) was used as the solver and META (v24.1.0) was used for postprocessing.

The material used in all SMC models were the material card MAT1 in OptiStruct is an isotropic elastic material [35]. The SMC material is assumed to be fully isotropic without taking the orientation of the fibers into account. In this model the data perimeters used is shown in Table 4.1.

Table 4.1: Material properties for the relevant CF-SMC used for the FE model.

Property	SMC
Young's Modulus Tension $[GPa]$	33
Young's Modulus Flexural $[GPa]$	25
Poisson's Ratio	0,33
Density $[g/cm^3]$	1,46
Tensile Strength $[MPa]$	120,5

During the first models the value used as Young's modulus was according to tension from the data sheet however the Young's modulus was later changed to the flexural modulus due to the material mostly experiencing bending in all objects. The strength limit used during evaluation was the one referring to tension due to it being the most conservative approach. The model was run as a non-linear geometry due to the high deformations during the loading and to capture the non-linearity of the material response.

4.1 Model Object 4

For object 4 the model was made in detail of the first sample from the first batch due to it being the first tested sample of the two available from object 4. The model was made of the 3D scanned geometry of the sample and measurements from the physical test. The model was made after the physical testing to compare the results when all were obtained.

4.1.1 Boundary Conditions

The load application was defined firstly as a rigid body element 2 (RBE2) which means that nodes chosen as slave nodes will be locked to have the same displacement as the chosen master node [36]. The master node is the node where the load will be applied. The load application position was measured from tests where the left application point was 18 mm from the radius and the right was 10 mm from the radius, see Figure 4.1.

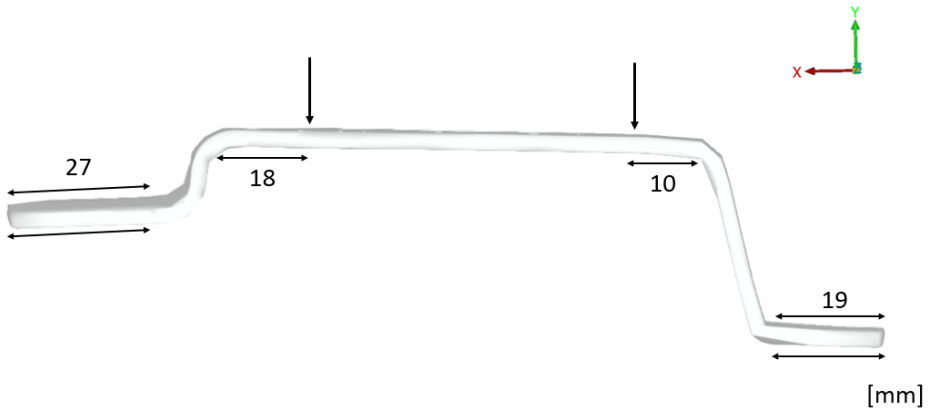

Figure 4.1: Schematic showing boundary conditions for object 4 where the measurements for the clamp's and load applicator's position are presented.

It was found that the model was too stiff compared to tests so in order to evaluate the impact of the load application cylinders from the test setup they were modeled too. The dimensions was 10 mm of each cylinder and they were modeled rigid. The connection between the cylinder and the test sample was a sliding connection. Which means that in every time increment the connection is reevaluated [37]. This was since the cylinders were sliding slightly in the physical test and a RBE2 connection was to stiff.

The clamped area where defined as a set of all nodes on the top and bottom surface of the sample to replicate the clamping of the fixture. The set was adjusted according to measurements from the test where the left had a clamping area of 27 mm and the right had a clamping area of 19 mm. The set included all sides where the sample was clamped, top and bottom on both left and right side. The set was later used to define a single point constraint (SPC) which was locked in all degrees of freedom. This made sure the clamped areas on the sample in the model was fixed as they were in physical test of object 4. In Figure 4.1 the measurements of each clamped area are shown.

4.1.2 Mesh

In order to capture the entire sample and the entire surface solid mesh was used. This was preferred since if a middle surface shell mesh was used the model would not be able to consider the surface of the sample. Since the data recorded from the GOM system were surface strain it is necessary to compare to a surface of the model, otherwise the comparison will not be accurate.

On the outside a shell mesh was made in order due to being able to extract surface strain. The mesh was a second order triangular elements (CTRIA6). In order to not have extra stiffness in the shell and for it to not add global stiffness the shell is set to the thickness of 0.001 mm and only the bending and transversal shear is set to 0 to not add extra stiffness. The size of the elements were 1 mm due to the thickness of the part being 3 mm and it is desired to have at least 3 elements over the thickness. As the solid mesh tetrahedral elements (CTETRA) were used. The size was 1 mm to keep having 3 elements over the thickness of the geometry. The cylinders were modeled with a shell mesh with quadratic elements (CQUAD4) with the mesh size 3 mm and solid elements which were hexagonal

elements (CHEXA) with the size as the CQUAD4 elements. The mesh on the sample can be seen in Figure 4.2.

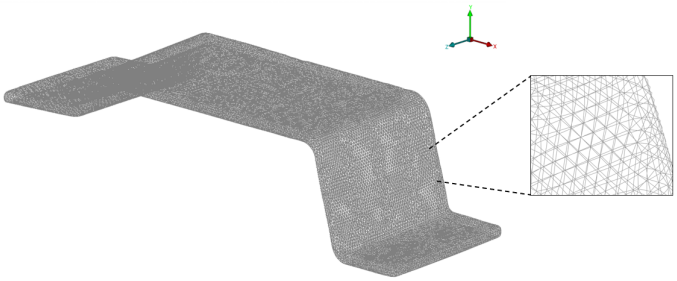

Figure 4.2: Figure showing the meshed object 4 with triangular elements outline presented as well as a zoomed in view of the elements.

4.2 Model Object 1

A detailed model was made similarly to the model described in Chapter 4.1 for object 1. Differently to the model for object 4, this model was done simultaneously as decisions about the test setup was being taken. Prior to any testing of the sample a model was set up, which is described in the following sections, and from this estimate critical force. After this the sample was set up according to the model and tested to 50% of the critical force and compared to the model, which was 75 N. This approach was taken in order to detect errors in the test setup prior to testing, hence not breaking samples unnecessarily.

4.2.1 Boundary Conditions

The clamped area was modeled with a SPC with the clamped area similarly to measurements taken from the physical test. The measurement of the clamped surface was 11.5 mm from the edge, see Figure 4.3. The SPC is locked in all degrees of freedom and the defined clamped area is the top and bottom of the sample.

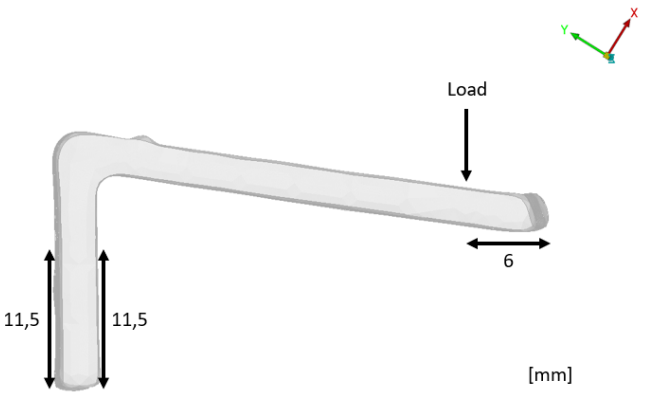

Figure 4.3: Schematic showing boundary conditions for object 1 where the measurements for the clamp's and load applicator's position are presented.

Load application was firstly done with a RBE2 however it was found to be a too stiff for modeling. In order to reduce the stiffness in the load application a RBE3 was introduced instead. An RBE3 is a rigid body element however the difference is that the nodes which are affected are allowed to move independently to the slave node however the same force is applied to them all [36] which is a more true representation of the test. The placement of the load was made according to measurements from physical tests. The boundary conditions can be seen in Figure 4.3. When building the model the load applicator was changed due to flexing in the load applicator assembly. The fixture was replaced with a solid aluminium piece with a triangular shape. Due to this the area which the load was applied to became slimmer and the sliding was less. See Appendix C for the test setup and load applicator.

4.2.2 Mesh

To capture the details from the 3D scanned sample a solid mesh was used and further it could be possible to extract the surface strain. A thin shell mesh was made on the outside of the sample for it to be possible where CTRIA6 elements were used. The size of the elements were 1 mm due to the sample thickness being 3 mm and wanted to have 3 elements over the thickness. The solid elements were CTETRA elements and $1mm$ in size. The meshed object can be seen in Figure 4.4. The load applicator was not modeled since it was assumed to not be sliding, which is described in Chapter 4.2.1.

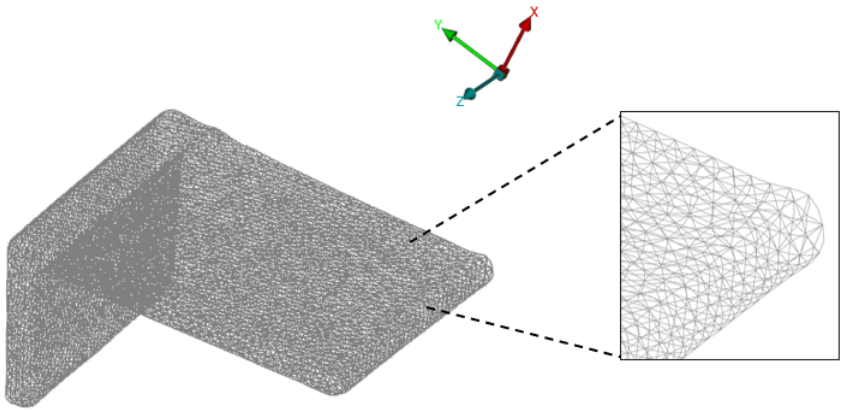

Figure 4.4: Figure showing the meshed object 1 with triangular elements outline presented as well as a zoomed in view of the elements.

4.3 Model of Stainless Steel Sample

It was seen that the correlation between the SMC FE models was poor, so a model and test was performed on a stainless steel sample since it has less complex material properties compared to the SMC samples. This was also a way to validate if the reason for the poor correlation could be the SMC material and samples or test.

The stainless steel sample was modeled similar to the procedure described in Chapter 4.2. The sample had the measurements and boundary conditions according to Figure 4.5. The material properties used for the model can be seen in Table 4.2.

Figure 4.5: Schematic showing boundary conditions for the stainless steel sample where the measurements for the clamp's and load applicator's position are presented.

Table 4.2: Material properties used for the stainless steel sample FE model.

Property	Stainless steel
Young's Modulus $[GPa]$	210
Poisson's Ratio	0,3
Density $[g/cm^3]$	7,8
Tensile Strength $[MPa]$	245

Three models were done to try and model the stainless steel sample to correlate the test. Firstly, a model similar to the one described in Chapter 4.2 was made with similar mesh and boundary conditions. Secondly, the same model as previously described was used however without the thin shell on the outside of the geometry in order to rule out if it added stiffness which resulted in an overly stiff model. Thirdly, a model was made with the middle surface of the stainless steel sample. In this model a mesh where CQUAD4 elements with the size 1 mm was used. See Figure 4.6 for the solid mesh and Figure 4.7 for the middle surface mesh. The load and clamping method was done as previously described with a SPC which locked the clamping area in all degrees of freedom and a RBE3 which represented the load application.

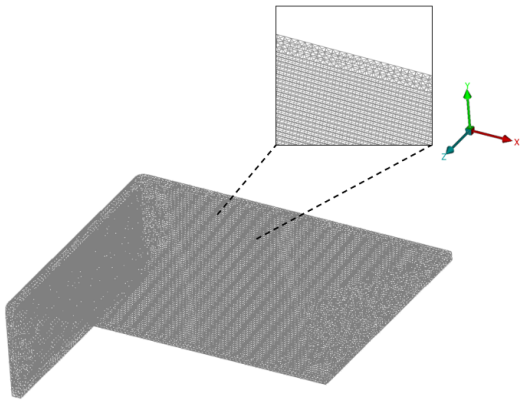

Figure 4.6: Figure showing the solid mesh for the stainless steel sample with triangular elements outlined as well as a zoomed in view of the elements.

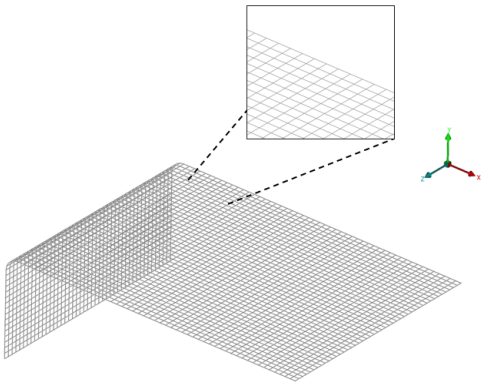

Figure 4.7: Figure showing the middle surface mesh for the stainless steel sample with quadratic elements and a zoomed in view of the elements.

4.4 Sensitivity Study

When doing the physical tests some differences will occur in clamping and load application due to human factors which needs to be taken into account when comparing the results. To evaluate how sensitive the FE model is to this a sensitivity study was performed. The model described in Figure 4.2 was used and four more models were done were the clamping area was moved up 1 mm and down 1 mm while keeping the loaded area in the same position. Next, the loaded area was moved 1 mm outwards and 1 mm inwards while keeping the clamped area the same. In Table 4.3 this is summarized.

Table 4.3: Summary of the different boundary conditions tested in a sensitivity study.

Test	Change
Clamped area moved upwards	1 mm
Clamped area moved downwards	1 mm
Loaded area moved outwards	1 mm
Loaded area moved inwards	1 mm

4.5 Evaluation

From the results of the models different things were analysed. First, a general visualisation was analysed in order to compare how the model deformed and moved compare to the tested videos and expected result. This is important to notice if something looks wrong, either in model or test setup. It is also good for the understanding of the model. From the model results a force-displacement curve could be plotted from the loaded node's force and displacement. This was then possible to directly compare to the data from the test machine from the tested samples.

Further, the principal stresses were analysed in the model to see the material response to the load. The principal stresses are useful in order to evaluate if tension or compression occurs in the expected area, and if any stress concentrations are present. The shear in the material was also analysed from the results, both in- and out-of-plane shear.

5
Results

The results from the material tests are presented in the Chapter 5.1 in the order they were tested. In Chapter 5.2 the results from the FE models.

5.1 Material Tests

The samples which were tested in the thesis were object 2, 4, 5 and one sample from object 1. The results from the tests are shown below in individual sections for each object. To be able to tell all samples apart they all had individual name using the following naming convention: B0X_O0Y_S0Z where B stands for what batch is is from and X is replaced which referred to batch, O for which object and Y is replaced which referred to object and S which sample and Z is replaced which referred to sample. As an example B01_O01_S01 is the first sample of object 1 from the first batch.

5.1.1 Object 2

Object 2 had in total four samples, two from each batch. A summary of the test results can be seen in Table 5.1 and in Figure 5.1 the force-displacement curve from each tested sample from object 2 can be seen. From the 3D scanned geometries there was a geometry difference between the batches which will in all likelihood affect the result. The difference can be seen in Appendix A. The first tested sample was tested twice with different results however the test setup changed from the first test done to all the rest, hence the Table is only referring to the adjusted setup. In the following sections the tested result is described in more detail. From the test it could also be seen that the critical displacement and force is the same point which the maximum displacement and force occurs for object 2.

Table 5.1: Test results from object 2 destructive testing where the critical displacement, critical force, maximum displacement, maximum force and failure mode is presented.

Sample	B01_O02_S01	B01_O02_S02	B02_O02_S01	B02_O02_S02
Crit. disp. [mm]	5.79	5.70	3.94	10.09
Crit. force [N]	410.45	295.49	269.82	354.52
Max disp. [mm]	5.79	5.70	3.94	10.09
Max force [N]	410.45	295.49	269.82	354.52
Failure mode	Interlaminar	Interlaminar	Interlaminar	Interlaminar

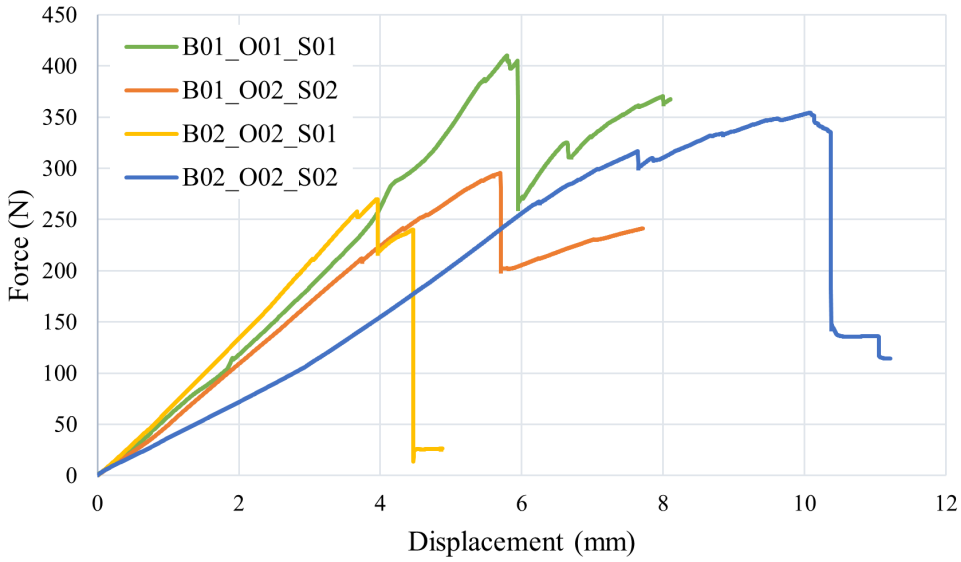

Figure 5.1: Force-displacement curve for object 2. Green curve is B01_O02_S01, orange curve is B01_O02_S02, yellow curve is B02_O02_S01 and blue curve is B02_O02_S02.

5.1.1.1 Thermography Scans

The pre-test thermography scans was made on all samples without any detected defects. The result can be seen in Appendix D. Due to unexpected results in the destructive testing a thermography scan was done again in order to detect any defects within the material. A picture from the scan can be seen in Figure 5.2. It can be clearly seen from the Figure 5.2 of the scan that a defect is detected inside the material. An exact determination of what type if defect is not possible but most likely it is a void due to the shape.

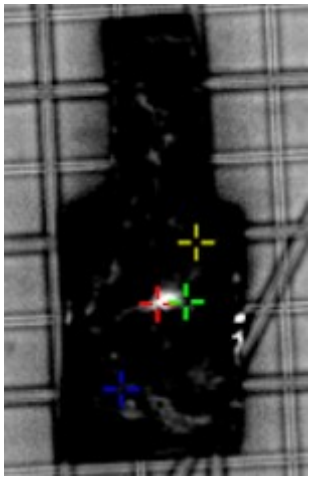

Figure 5.2: Thermography scan post-testing for B01_O02_S01 where a light area can be seen in the middle of the sample which is interpreted as a void inside the material.

5.1.1.2 Destructive Testing

The sample, B01_O02_S01, was first tested with the original setup which resulted in a interlaminar failure along the flat part in the sample between the radii, see Figure 5.3. From the model a failure was expected in the lower radius and a high sensitivity to the

radius which could not be seen in the test. As mentioned from theory the crack had a stopping motion, not a smoothly propagating crack, which is because of the load transfer between the fiber chips in the material. During the test the load fixture was sliding when applying the load which resulted in a constantly moving load application and the most loaded area on the sample was moving along the sample which was not predicted in the model and resulted in two different results. In order to control this movement, the clamped area was moved further up on the sample which stabilised on the flat surface between the radii. A new test was run on the first sample and it again failed interlaminarly and not in the radius, see Figure 5.3 and Figure 5.4 for the crack initiation position.

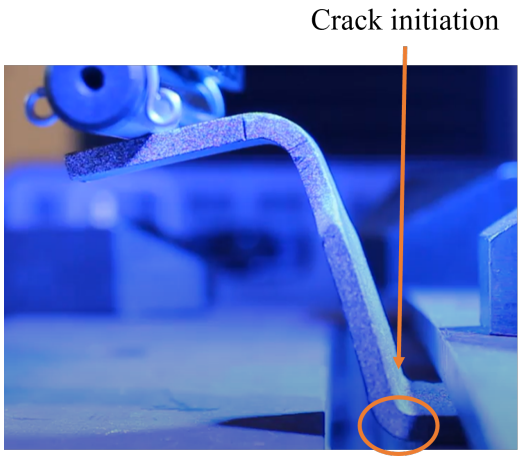

Figure 5.3: Object 2 in the original test setup and clamping with the crack initiation location marked with an orange circle.

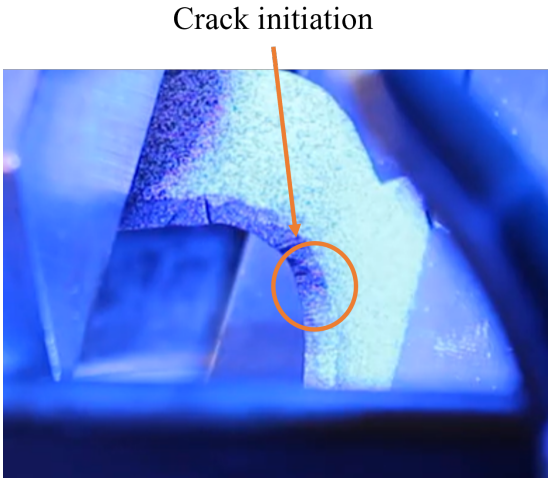

Figure 5.4: Object 2 in adjusted test setup with changed clamping with the crack initiation location marked with an orange circle.

The remaining three samples were tested with the later setup with a higher clamping position. All samples failed similarly to the first sample with interlaminar failure and not in the expected radius. The crack initiation of all samples were changing in position but they did not seemed to be very sensitive to the radius, however the same stopping motion noticed from th first sample could be seen on all samples.

5.1.1.3 Strain Measurement

Due to the sample not fracturing in the expected area in the first test of B01_O02_S01 the strain mapping system was not aimed at the fractured surface. However, it shows the result from the material under loading which is still interesting results. These results were not analysed further.

5.1.2 Object 4

For object 4 there is one sample per batch and the test results is described further in the following sections. In Table 5.2 a summary of the results from destructive tests are shown and in Figure 5.5 the two tested results are plotted.

Table 5.2: Test results from object 4 destructive testing where the critical displacement, critical force, maximum displacement, maximum force and failure mode are presented.

Sample	B01_O04_S01	B02_O04_S01
Crit. disp. [mm]	3,33	3,46
Crit. force [N]	2677,02	3082,82
Max disp. [mm]	5,31	4,58
Max force [N]	3199,83	3408,49
Failure mode	Interlaminar	Interlaminar

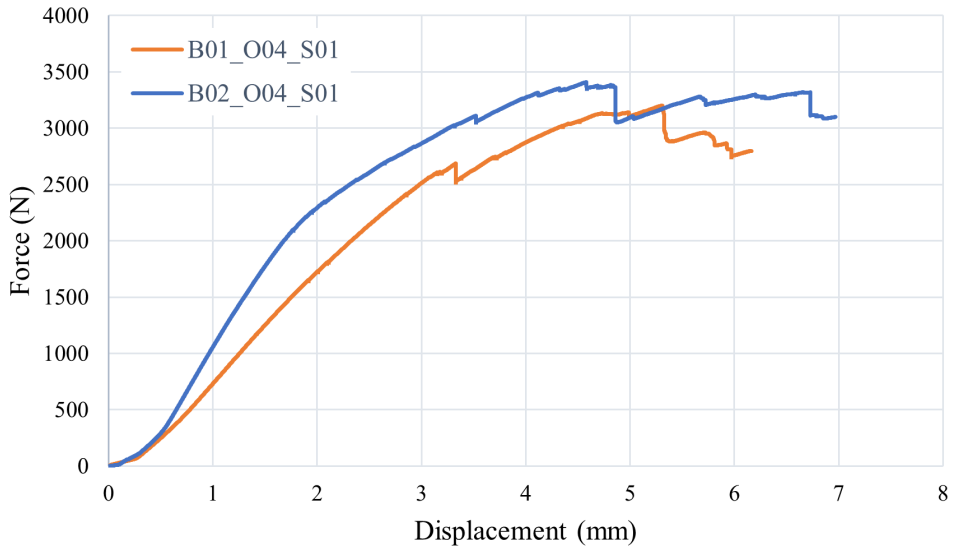

Figure 5.5: Force-displacement curve for object 4. Red curve is B01_O04_S01 and blue curve is B02_O04_S01.

5.1.2.1 Thermography Scans

The pre-test thermography scan of the two samples were done and in neither of the samples any defects could be found. Due to no indication of defects prior to the test and both samples failed in similar manner no post-thermography test was done on object 4. Result from thermography scan can be seen in Appendix D.

5.1.2.2 Destructive Testing

From the destructive testing of object 4 the two samples have similar results. Similarly to object 2, object 4 did not have crack initiation in the expected area. Both samples had crack initiation between the load applicators, instead of the radius which was expected to be the critical area from the original model. The sample B01_O04_S01 had

crack initiation from the edge of the sample and then had a interlaminar failure. Sample B02_O04_S01 has similar failure mode as the sample B01_O04_S01, interlaminar failure with a crack initiation between the load samples. Position of the crack initiation on both samples were in a position where the deformation is high. See Figure 5.6 and Figure 5.7 for pictures from test of sample B01_O04_S01 and B02_O04_S01 respectively.

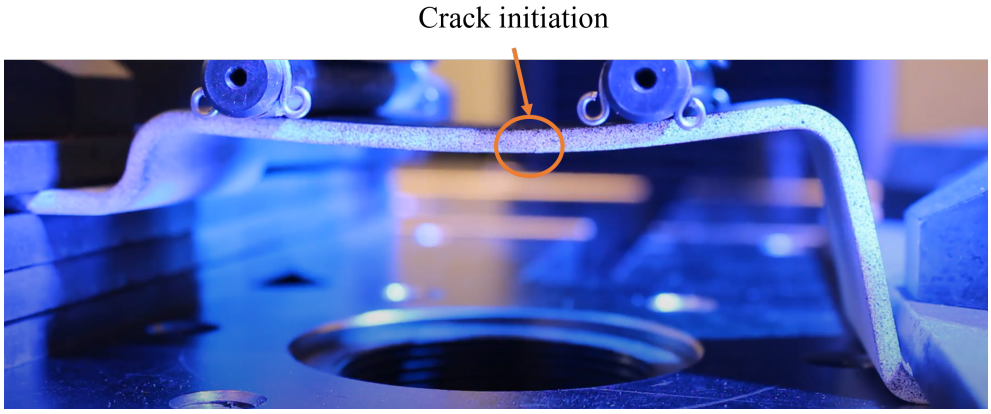

Figure 5.6: Crack initiation point for B01_O04_S01 shown in orange circle.

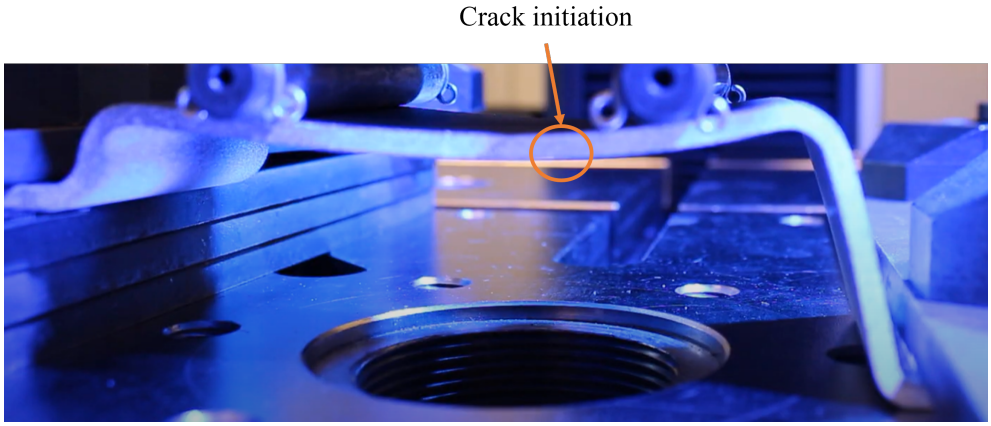

Figure 5.7: Crack initiation point for B02_O04_S01 shown in orange circle.

It was later found out that the load application assembly used in this test, seen in Figure 5.6 and 5.7 as the two cylinders on top of the sample, was deflecting when loaded. This made the test result unreliable.

5.1.2.3 Strain Measurement

Due to the failure not being in the area expected the strain mapping system where not aimed at the surface where the crack initiated. This then resulted in not capturing the fracture at all of object 4 in the GOM system however, the data can still be useful due to the elastic response of the material. The data was however not analysed further.

5.1.3 Object 5

For object 5 the there were three samples on each batch which resulted in a total of six tested samples. One of the samples, B01_O05_S02, had a crack and broken edge before

the test were conducted which gives a stress concentration during loading, the crack on the sample can be seen in Appendix B. This made the sample B01_O05_S02 difficult to use in further analysis comparing FE model to test data. Moreover, the jig used for all object 5 destructive tests were deflecting during loading which leads to unreliable results. Moreover, some samples were slipping in the clamped fixture during the tests. With this in mind when looking at each of object 5, they all were ruled out as objects to model in a greater detail. In the Tables below the results from the tests can be seen with Batch 1 in Table 5.3 and Batch 2 in Table 5.4 respectively.

Table 5.3: Test results from object 5 destructive testing, batch 1. The critical displacement, critical force, maximum displacement, maximum force and failure modes are presented.

Sample	B01_O05_S01	B01_O05_S02	B01_O05_S03
Critical displacement [mm]	4.05	7.09	7.61
Critical force [N]	935.29	3038.02	2288.84
Maximum displacement [mm]	9.69	3.61	10.50
Maximum force [N]	925.87	3038.02	2571.90
Failure mode	Interlaminar	Interlaminar	Interlaminar

Table 5.4: Test results from object 5 destructive testing, batch 2.The critical displacement, critical force, maximum displacement, maximum force and failure modes are presented.

Sample	B02_O05_S01	B02_O05_S02	B02_O05_S03
Critical displacement [mm]	6.46	6.21	5.82
Critical force [N]	3226.19	3452.69	2544.78
Maximum displacement [mm]	9.81	8.6241	9.70
Maximum force [N]	4070.45	3741.96	3720.23
Failure mode	Interlaminar	Interlaminar	Interlaminar

5.1.3.1 Thermography Scans

Pre-test thermography scans were made and they did not reveal any defects and this resulted in no post-test thermography scans. See Appendix D for thermography scan pictures. A post-test thermograpgy scan was not done due to the tested results not trusted due to the setup or the sample had surface defects from the start.

5.1.3.2 Destructive Testing

As mentioned previously, there were multiple errors during the destructive testing of object 5 and this resulted in unreliable test result and a summary of the errors during the test can be seen in Table 5.5. However, it was useful information from the tests that the failure was interlaminar failure on all samples from object 5. They started around the predicted area on the samples although all four samples had a crack initiation and propagation interlaminarly. In Appendix B pictures of all tested samples can be seen.

Table 5.5: Errors during testings on object 5 samples for different samples.

Sample	Errors
B01_O05_S01	Fixture flexing and broke around clamp.
B01_O05_S02	Fixture flexing, damaged edge and sample slipping in fixture.
B01_O05_S03	Fixture flexing and broke around clamp.
B02_O05_S01	Fixture flexing and premature crack propagation.
B02_O05_S02	Fixture flexing and failure initiation not visible on camera.
B02_O05_S03	Fixture flexing and damaged edge.

5.1.4 Object 1

Since the model and test was done simultaneously the sample was only tested until 50% of the critical force. The test was only done on the sample B01_O01_S01 and it was done multiple times in order to validate the test setup. In Figure 5.8 a graph is shown of tested result. Only one sample were tested and not until failure so the critical displacement and force is not known.

5.1.4.1 Thermography Scan

All samples were pre-test thermography scanned and no defects could be found in the samples. Since no sample was tested until failure and no unexpected failure and no need was seen to do any further thermography scan tests. See Appendix D for the result.

5.1.4.2 Destructive Testing

The sample was only tested to 50% of the predicted critical force and not until failure so the critical displacement and force was not known however some results meant that the test setup changed. In Figure 5.8 the original test result can be seen as the orange line. As can be seen in the Figure the result is not linear at all and it seems to have a plateau in the graph at around 0.8 mm of deformation which is not an expected behaviour. It was noticed that the clamps holding the cylinder in the load application assembly moved and shifted the cylinder in the middle of the test which can be assumed to be what is seen in the force-displacement graph in Figure 5.8 hence the load application were changed. A new test was performed and the result can also be seen in Figure 5.8. Here it can be seen that the response is linear and the unexpected plateau can not be seen. This indicates that the setup does not have any slipping or unexpected movement during the test.

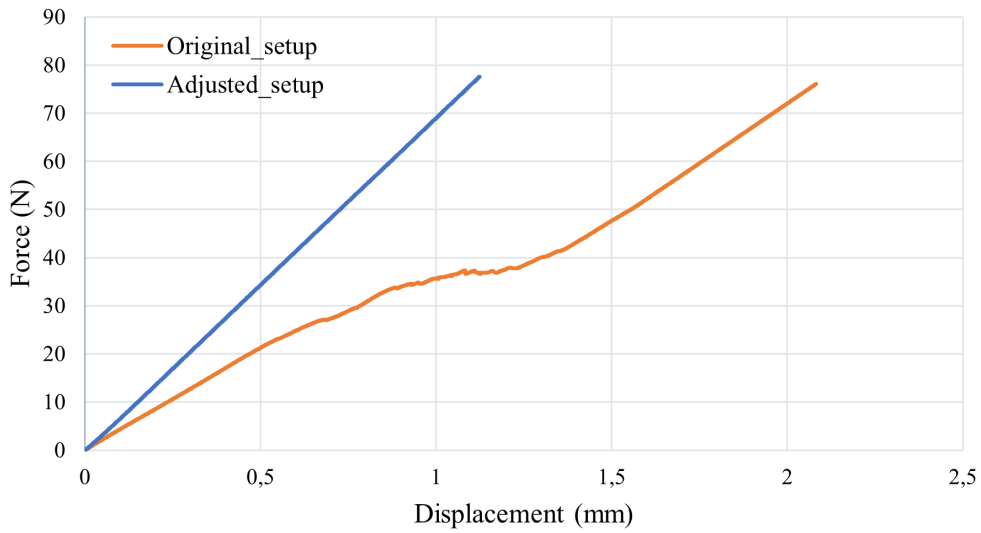

Figure 5.8: Force-displacement curve for object 1. Orange curve is first test with original setup and the blue curve is the adjusted setup.

5.1.5 Stainless Steel Sample

The stainless steel bracket were tested in the same setup as object 1. The sample was tested to 75 N as for to test similarly as object 1. To validate the clamping method two clamps were used and both results can be seen in Figure 5.9. See Appendix C for the load applicator.

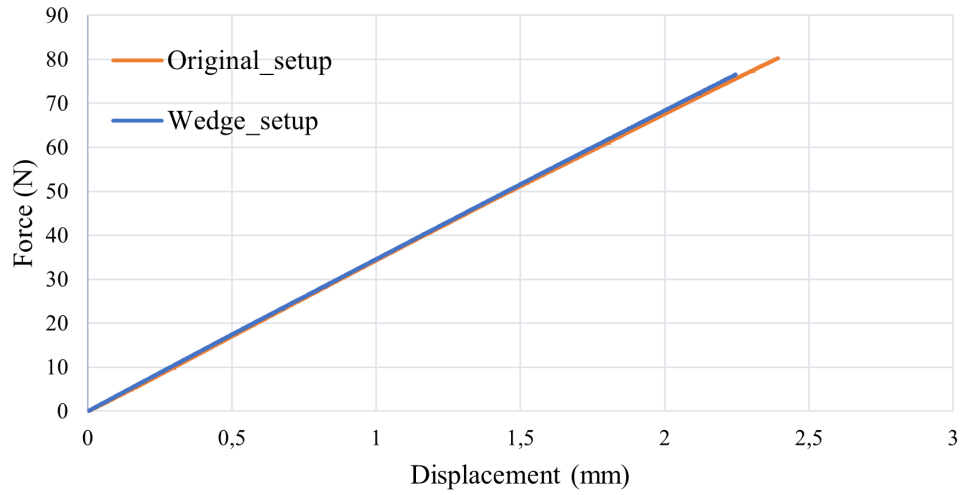

Figure 5.9: Force-displacement graph showing the two different plots of the two setups. Original setup is orange and blue is the wedged setup.

As can be seen from Figure 5.9 the difference between the two clamping setups were small and therefore the original setup and clamping method was deemed usable.

5.1.6 Validation Results

From the validation test done to make sure the displacement recorded by the machine was accurate it was found that the error between the two measurements were $1,5\%$. In Figure

5.10 the two measurements are plotted in order to see the different results. The plot shows the Force-Displacement curves. This was deemed to not be affecting the results in any noticeable size. A validation test if the test machine's recorded data was accurate. The result was the same from the recorded displacement and the manually measured.

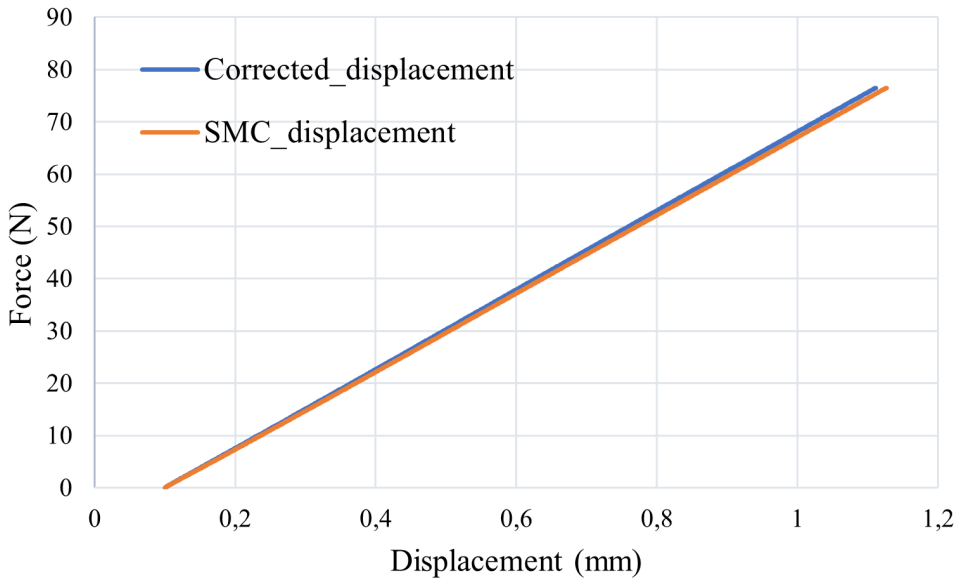

Figure 5.10: Force-displacement graph showing the two different plots from the validation test. Corrected displacement is blue and orange is the displacement from the SMC.

5.2 FEA Results

The FEA results are divided in objects, steel plate and sensitivity study. It can all be seen in the following sections.

5.2.1 Object 4

For object 4 it was first modeled with an RBE2 as a load application and later with the cylinders modeled from the test setup with a slide contact between the cylinders and the object. In the model the force and displacement taken as a result for the force-displacement curve was the point where the load was applied as it is in the collected data from the test machine. The results from the RBE2 and cylinders with slide contact can be seen in Figure 5.11.

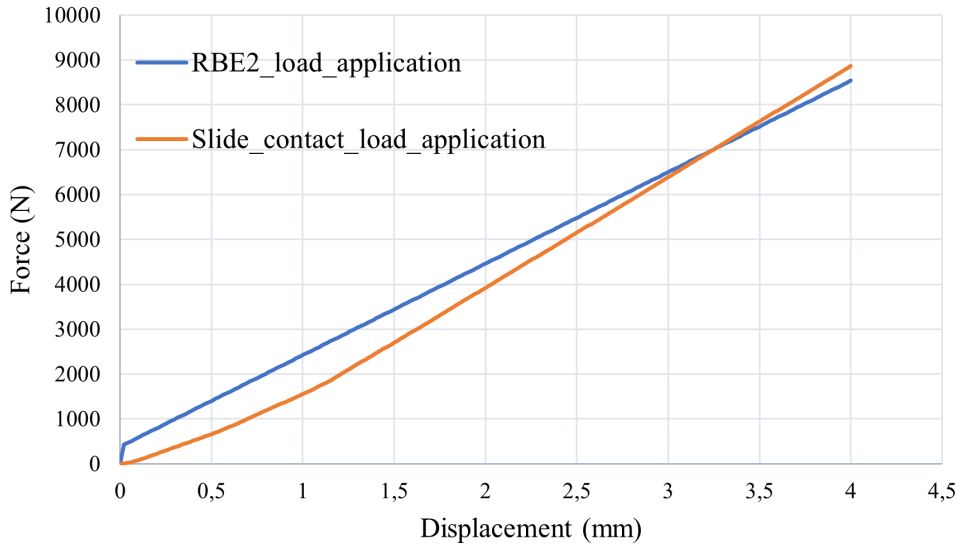

Figure 5.11: Force-displacement graph comparing the load application with RBE2 (blue) and a slide contact (orange).

To look at the results from the model of object 4 the geometry was split in two places to compare the results in the top radius and between the load applicators. This is due to the top radius, section B, is the critical area in the model. The middle of the load applicators, section A, is where the sample had the crack initiation in the physical test. The sections can be seen in Figure 5.12 and are referred to as A and B.

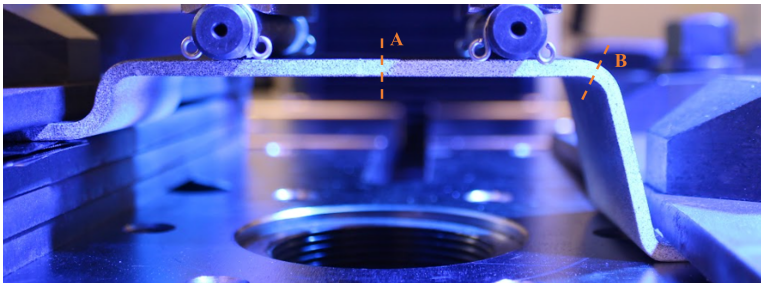

Figure 5.12: Figure showing the two split section labeled A and B where A is located in the middle of the sample around where the sample had is crack initiation and B in the radius to the top right due to it being predicted to be the most loaded region.

In Table 5.6 a summary of the values from the model can be seen. The results shown are displacement, stress on the top and bottom side, in- and out-of-plane shear taken from the sections A and B shown in the Figure 5.12. The values are taken from when the sample starts to fail in the model, the stress reach 120 MPa.

Table 5.6: FEA results from object 4 at failure from section A and section B. The displacement at load application, stress top side, stress bottom side, in-plane shear and out-of-plane shear is presented.

Results	Value Section A	Value Section B
Displacement at load application [mm]	0,57	0,05
Stress top side [MPa]	25,3	65,9
Stress bottom side [MPa]	24,1	120,2
In-plane shear [MPa]	2,1	50,5
Out-of-plane shear [MPa]	9,7	12,9

From the model the area which fails first is the lower side of the radius at Section B. In the model the sample is most sensitive to compression as the most loaded area is experiencing. The shear, both in- and out-of-plane is significantly lower from the model compared to the stress, both experienced in compression and tension.

In Figure 5.13 a comparison between the model's force-displacement graph and the tested graph can be seen. It is clear from the result that something is not captured correctly in the model och something in the test is not correct. It was later found that the load applicator assembly had moving parts, as mentioned in Chapter 5.1.2.2.

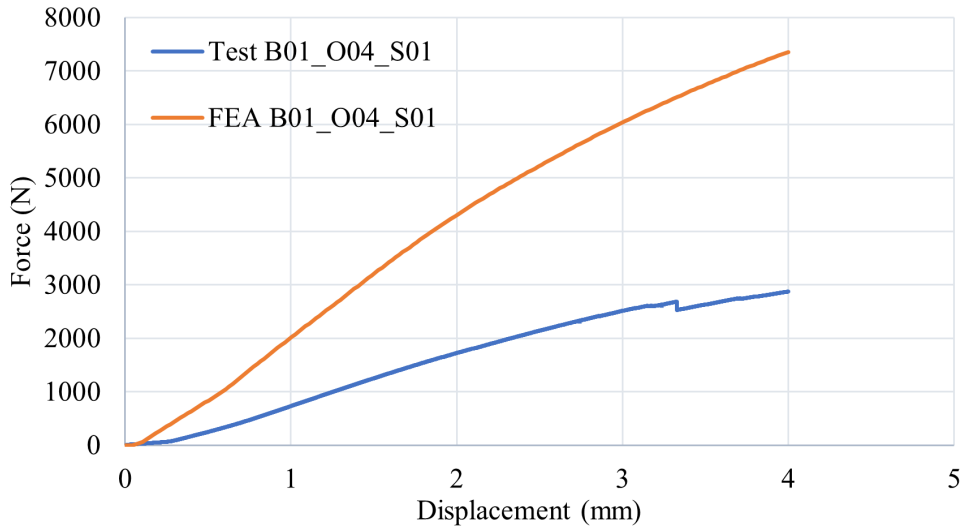

Figure 5.13: Figure plotting the force-displacement curves for the FEA (orange) and the tested result (blue) for object B01_O04_S01.

5.2.2 Object 1

For the model of object 1 two different once were made with either a RBE2 or RBE3 as a load application. The difference in the force-displacement curve can be seen in 5.14. It can be seen a significant difference between the two load application methods and the RBE2 is stiffer. The RBE3 was used as a load application moving forward.

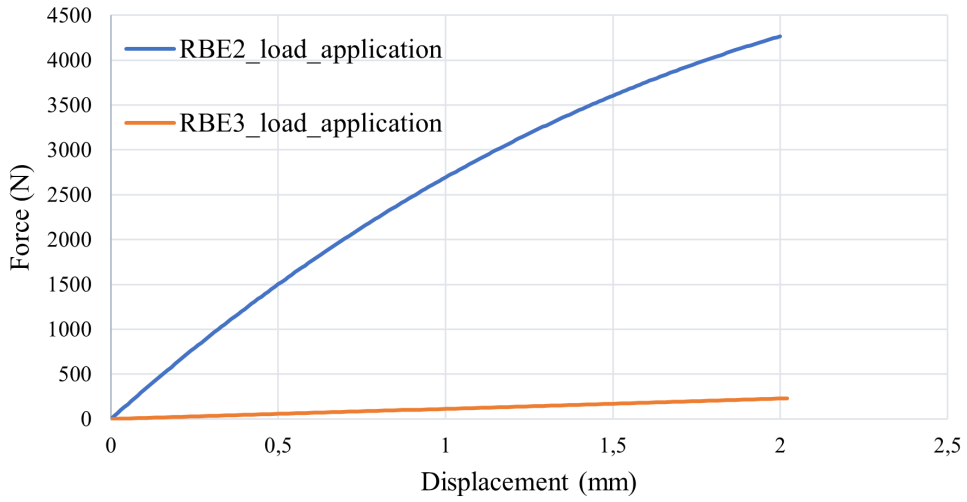

Figure 5.14: Figure showing the difference in a force-displacement graph, the RBE2 is the blue line and the RBE3 is the orange line.

From the model result principle stress, in- and out-of-plane shear was obtained and the result is summarized in Table 5.7. The values were taken from the radius of the sample since it is the most loaded area and there for also the most critical part. The section can be seen in Figure 5.15 and the section is referred to as A.

Table 5.7: FEA results from object 1 when 75 N applied and failure. The displacement at load application, stress tensile side, stress compression side, in-plane shear and out-of-plane shear is presented.

Results	Value 75 N	Value Failure
Load [N]	75	226
Displacement at load application	0,6	1,2
Stress tensile side [MPa]	52	100
Stress compression side [MPa]	45	120
In-plane shear [MPa]	0,9	1,7
Out-of-plane shear [MPa]	1,9	1,8

In the Table 5.7 the values are first from 75 N load due to it being the the tested value and further until failure in the FE model. The model seems to be most sensitive to compression. In the model, the shear is very low compared to the tensile and compression stress. This results in that from the model the sample will most likely fail on the compression since of the sample due to compressive stress.

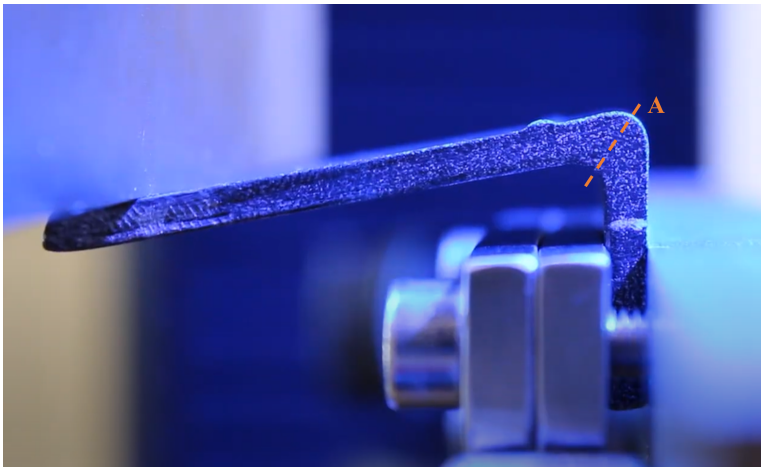

Figure 5.15: Figure showing the split section A in object 1. It is positioned in the radius due to it being predicted to be the most loaded region.

5.2.3 Stainless Steel

The stainless steel bracket was modeled in three ways as described in Chapter 4.3 and the force-displacement curve can be seen in Figure 5.16 where all three results can be seen.

From the force-displacement the two solid models from the 3D scanned geometry have similar results which means the shell mesh on the model does not add any significant stiffness. The shell model of the middle surface was stiffer which can be seen in the Figure 5.16.

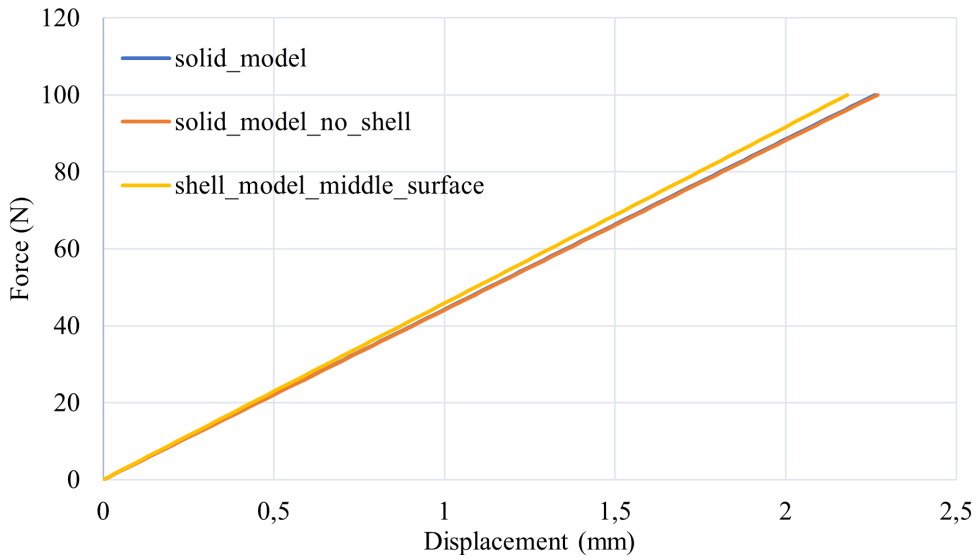

Figure 5.16: Force-displacement curve for three model of stainless steel sample. Blue line is the solid model, orange is the solid model with no shell elements and the yellow is the model with only shell elements and made from the middle surface.

Moreover, the model was compared to the tested result from the stainless steel bracket. The force-displacement curve from the test and the model was compared and the result can be seen in Figure 5.17.

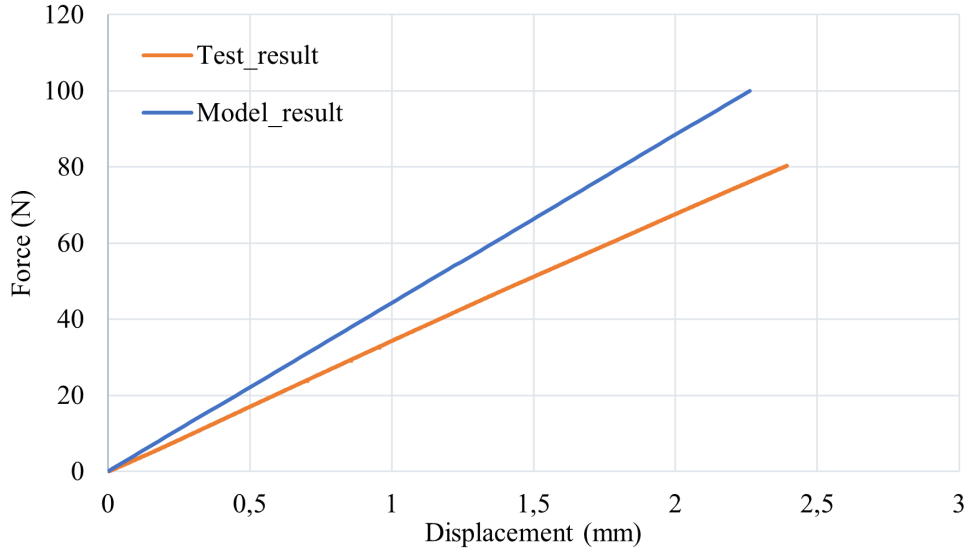

Figure 5.17: Graph displaying the difference between the model and test for stainless steel sample in a force-displacement curve. The blue line is the FE model and the orange is the tested result.

The model and test are not correlating as expected and the model is stiffer by a factor of 1.3 which is more than expected from a model with stainless steel.

5.2.4 Sensitivity Study

A sensitivity study was done on the model for object 1 to see how sensitive the model was to changes in the setup. Firstly, for object 1 the force-displacement graph can be seen in Figure 5.18. The model was done to check the sensitivity of the clamped area by moving it up and down 1 mm and the sensitivity to load application position by moving it in- and outward by 1 mm.

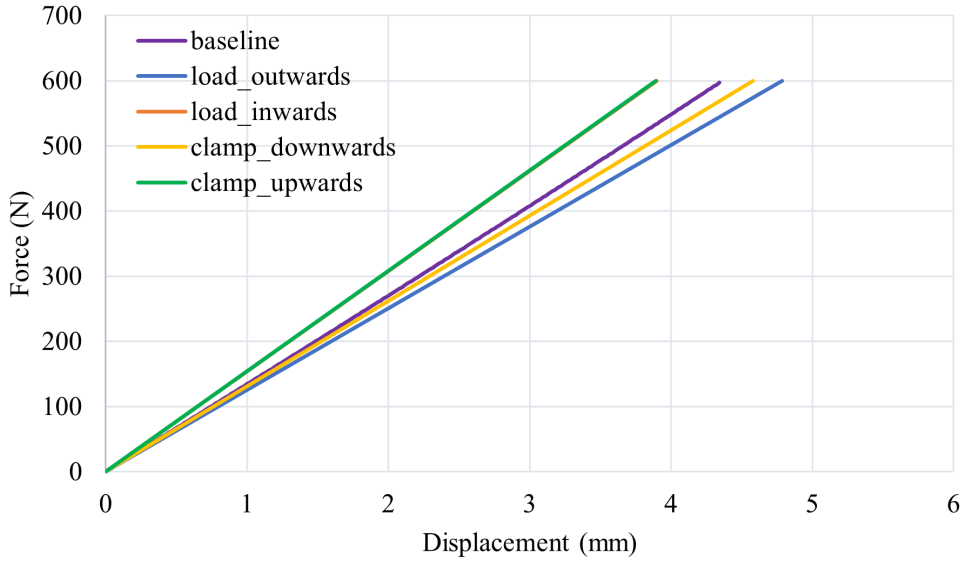

Figure 5.18: A graph showing the result from the sensitivity study done on object 1. Baseline is displayed in purple, the load moved 1 mm outwards is green, the load moved 1 mm inwards is orange, the clamped moved downwards 1 mm is yellow and the clamped moved upwards 1 mm is green.

The model does not deviate so much from the baseline and the biggest error to the base line is when the load application was moved 1 mm outwards and the error to the baseline was around 10% which is not significant compared the the error towards the tested result shown in Figure 5.17.

6
Discussion

Comparing material tests to FE model can be a complex procedure due to many variables are difficult to control. In this thesis it becomes clear that many unexpected problems can affect the result and vice versa, not everything expected to be a problem was. First of all, a composite is dependent on the structure of the fiber and matrix for its strength and stiffness. For SMC the fibers are short and randomly distributed in the material which makes it quasi isotropic if everything is correct in the samples. One concern which was raised, and was partly the background for the thesis, that the material was weaker in small radii and ribs which needed to be investigated. In the following sections a discussion regarding the material tests and correlation between the FE model and test results.

6.1 Test Results

From the material tests a sensitivity to small radii were not experienced, but rather that the material and geometries were more prone to interlaminar failures than failures in a radii. From all the tests done in this thesis the samples had interlaminar failures. Note that all samples were loaded in bending which makes the risk for interlaminar failure greater. However, it could not be seen that the samples were specially sensitive to the radii in the samples. Nevertheless, even though the samples did not fail or seem sensitive to the radii this does tell anything about how the fibers are distributed. None of the test methods in this thesis provided any information regarding the fiber distribution and it is not possible to say how the fiber content looks over the sample. However, as mentioned the samples did not seem to be so sensitive to it but rather prone to the interlaminar failure modes.

Moreover, multiple errors where discovered during the physical testing from the samples and objects. This resulted multiple test results could not be used in a comparison with an FE model. For object 2 and 5 the tested results were ruled out as a comparison to an FE model due to slipping and flexing testing fixtures. For object 4 the model was made prior to finding out problems in the load application assembly which is the reason for the model being done and the result later decided to be unreliable. Of the tested elements only object 1 was left as a possible test to correlate an FE model to. Due to this, only one test sample remained which is not ideal since the more samples which are tested the better security can be found in the behaviours from the results.

It can be seen across all objects that the difference from the tests between the samples within the same object are quite significant, this can be seen on the force-displacement graphs in Chapter 5.1. This can suggest that the strength of the same material in similar geometries varies. Even though most samples did not seem to have defects within the material from the thermography scans it could indicate defects which were missed or not

detected. It could also indicate fiber content change in areas which are loaded, such as radii, which can not be confirmed but it could be a possible explanation for the behaviour. However, as mentioned previously none of the tests had a failure initiation in a radius which suggests that the material is not sensitive to radii. Another possibility is that the sample is placed differently in the test fixture or other differences in the physical setup which can affect the end result. From the sensitivity study for object 1, see Chapter 5.2.4, the model was not sensitive to the setup changing however that could be a reason for slight change between different samples having different results regarding the force-displacement graphs of the tested objects. Moreover, The samples were manually cut out by hand hence differences between the samples are a high likely. From object 2, see Appendix A, the differences between the batches and the differences in geometry are quite significant in the top radius which is expected to be a heavily loaded area which could be some explanations to some of the differences in the force-displacement graphs.

Due to modeling result and test results not correlating from object 1, see in sections below for discussions regarding the FE model and correlation, the stainless steel sample was tested. The sample was as mentioned tested to 75 N as the SMC object 1 sample was tested to and two tests were done in order to validate the test setup. From the validation test the clamping setup was tested and since it gave similar result it does not seem to be one a source of error. Further, the validation test done on the machine in order to see if the detected the true displacement also gave valuable results to rule out sources of error from the machine and test setup.

6.2 FE Model Results

An FE model is an approximation of what is the expected result from the tests and the more detailed it is it often gets results closer to reality however it also takes a significantly longer time and more computational power which is always a balance. The model for object 4 was done with a slide contact in order to be able to capture the loads movement which was needed to not have an overly stiff model as was seen from using RBE2 as a load application. However, this makes the model more complicated and takes longer to run. For object 1 the model, the interaction was not done using a sliding contact due to or not seeming to slide as it was for object 4 from the load application in the test. The stiffness close to the added RBE3 in object 1 is expected to be too stiff however that is not the region which is analysed and therefore it was deemed to be an okay approximation. For object 4 the area close to the load application is more vital due to the failure happening relatively close which is one reason more to model with a slide contact and modeling the load applicators. In object 1 the maximum loaded region is expected to be the radius, however since the test was not run until failure, if that would be the failure initiation point is not possible to say. However, if only the elastic response is taken into account the model was overly stiff and a significant difference between the modeled force-displacement curve and the tested curve. No errors could be found in the model nor the test and this implies that the sample has defects which could not be seen from the thermography scan, this further lead to the investigation of the stainless steel sample in order to be able to see if the sample could be the problem.

Since the FE model is much stiffer in all cases there is a possibility the material SMC is modeled too stiff. The material card used to describe the material in the model is assuming

it is a fully isotropic material which is not fully accurate but rather an approximation. The SMC is expected to be isotropic in the plane but out of the plane it is not going to be due to the layers of fibers being in one plane from the manufacturing. Since the samples broke through interlaminar failure it can be a possibility that the material experiences more out-of-plane loads than predicted in the model and therefore is less stiff compared to the model. This could be one explanation for the model being too stiff. However, this does not explain why the stainless steel sample is too stiff in the model since this is an isotropic material and the material model should not be inaccurate the same way it has a possibility to be that regarding the SMC.

In order to validate if it is the SMC sample which was problematic and not modeled correctly or if the error comes from another issue a stainless steel sample was modeled and tested. The steel sample has less complex material properties and due to this a lower error, between the FE model and the tests, was expected compared to the SMC model. A lower error compared to model for object 1 was achieved but not as small as expected.

6.3 Correlation Between FE Model & Test Results

The correlation between the material tests and FE models are significantly lower than expected from all tests and models. Many reasons could play a role into that results, both from the test setup or the FE model setup. As mentioned multiple problems were found during the testing of the samples which had to be adjusted and the possibility for more problems exists however to what extent is not possible to judge. Due to the validating tests done however, the more clear or obvious sources of error has been validated from the test. To correlate an FE model to a test as close as possible to a perfect setup is needed from the physical testing. Some difference is expected as some degree of slipping at the clamping position, fixture flexing or load application moving is always present and an FE model is an approximation for what happens. Keeping this in mind a small deviation is expected however the degree of difference in all models and tests done in this thesis is more than expected.

In all likelihood the error might be depending on multiple different factors as mentioned previously. In order to determine the cause a deeper study is needed on the test procedure, investigation of the samples and evaluation of the contents in the FE model. Since the validation test setups, sensitivity model and general overlooking of the work have been done the source of the deviation is unknown and a potential cause is not known.

7
Conclusion

The aim of the thesis was to investigate how the geometry affects the properties of the material and correlate FE models and material tests. From the work done in the thesis the material tests were analysed and many sources of error were found in the test setup for example how the sample was clamped and the load applicator assembly was constructed. This resulted in many test results not being possible to use in comparison to an FE model. Further, the models and material tests did not correlate as expected and the model is overly stiff in comparison to the physical tests. Due to the time limitations in the thesis the DIC result was not used for mapping the strain and comparing to the FE models. Further, the constituent tests were not possible to do within the timeframe of the thesis either. The main conclusions from the thesis can be seen below.

- The material strength does not seem to be relatively sensitive to radii in the geometry. No samples had a crack initiation in a radius but they were however more prone to interlaminar failures which was not expected.
- The FE material model is overly stiff and either the load application, clamping system or material representation is stiffer than reality.
- The correlation between the FE model and test is not as accurate as expected prior to the thesis start. The reason why the FE model is stiffer is not clear and more investigation is needed of the FE model as well as ruling out eventual issues from the physical tests.

8

Future Work

Since the results were not as accurate as expected throughout the thesis there are multiple things which can be done to reach a more accurate result and a more through investigation if the reason behind the results. In this chapter some possible next steps are described and the importance of them.

Regarding the material tests some evaluation could be done in order to rule out eventual errors. Since a couple validation tests have been done on the machine and its deformation recording as well as the two clamp setups used for the stainless steel sample it did seem to validate the test. However, during a material test there is always some movement and there is a possibility that both the clamps validated against each other had similar problems or possible flexing or slipping. Further, there is a possibility that there is more compliance in the test machine as first was thought of. To investigate the flexibility in the test setup the GOM system could be used to evaluate the deformation of the load applicator and the clamping system. This should give an better evaluation on how big the compliance is in the test setup.

In order to evaluate the fiber content distribution over the samples some different approaches could be used. Computed Thermography (CT) scans is a non-destructive testing technique were it is possible to map out the fiber directions and further also the fiber and matrix distribution over the sample. This could be of big importance to know when the distribution of the fibers are to be taken into account in the model or in order to evaluate how the material behaves in radii or ribs. Another method which can give the fiber and matrix content is to do a constituent content test. This is when a part of the sample is weighed as a whole, then the matrix is burnt of and lastly the remaining fibers are weighed. This way the weight distribution between the constituents can be found in the investigated areas. This can be done on the most critical areas and least critical area to have a reference. A recommendation could be to make one test in a radius of a sample, where failure initiated and somewhere as far away from either as possible in a non-critical area. This would give the possibility to investigate if the fiber content might be varying over the component and if any critical features could be a course for changing fiber content.

Further, it was discovered that all samples broke through interlaminar failure which is interesting. What this can suggest is that the in- and out-of-plane stress and strain can be important to analyse in the material. The load transfer inside the material can have a great importance and for a future step this should be investigated. Both from a material point of view on how the material reacts to interlaminar loads as well as how the load transfer might be affected due to the material structure and geometrical features. Also from a analysis perspective, analyse the FE models in way to see if this can be captured and how it might affect the structural integrity of the part or sample.

One possibility to model the material more accurately is to not use the assumption of fully isotropic material which was done in the thesis since it is not but rather a quasi-isotropic material. To do this accurately more information would be needed of the material such as how many layers were used in manufacturing. What could be modeled is that all layers have isotopic behaviour and then these layers are stacks on top of each other, this would give a different material response mainly out of plane. The stresses between the layers would not be possible to capture this way since all layers have the same properties however the out of plane properties will be different and closer to reality rather than the currently assumed isotropic. How much this can affect the result is difficult to say.

As a last recommendation is to test the material with less complex shapes. Firstly, start with doing simple tensile and 3- or 4-point bending tests in order to validate the material data which the FE model is based on. Moreover, investigate if there are possibilities to take similar samples for tensile and bending tests from more challenged areas due to radii for example. To tests both there types of samples it would hopefully be simpler to model and test due to it being a conventional testing method. This could be a way to validate the material data used as well as evaluating if the material behaves better or worse if the samples are taken from different parts of the part since the radii are expected to have worse properties.

Bibliography

[1] K. Dilip Kumar et al. "Morphological and mechanical properties of short fibres reinforced hybrid composites for automotive applications". In: *Materials Today: Proceedings* 52 (Jan. 2022), pp. 957–962. ISSN: 2214-7853. DOI: 10.1016/J.MATPR.2021.10.401.

[2] Fardin Khan et al. "Advances of composite materials in automobile applications – A review". In: *Journal of Engineering Research* (Feb. 2024). ISSN: 2307-1877. DOI: 10.1016/J.JER.2024.02.017.

[3] M Oldenbo. *Anisotropy and non-linear effects in SMC composites From material data to FE-simulation of structures*. Tech. rep. 2004.

[4] Zhangxing Chen et al. "Failure of chopped carbon fiber Sheet Molding Compound (SMC) composites under uniaxial tensile loading: Computational prediction and experimental analysis". In: *Composites Part A: Applied Science and Manufacturing* 118 (Mar. 2019), pp. 117–130. ISSN: 1359835X. DOI: 10.1016/j.compositesa.2018.12.021.

[5] P.K. MALLICK. "Particulate and Short Fiber Reinforced Polymer Composites". In: *Comprehensive Composite Materials* (Jan. 2000), pp. 291–331. DOI: 10.1016/B0-08-042993-9/00085-1.

[6] Michael F Ashby. *11.4 Composites*. 2011. URL: https://app.knovel.com/hotlink/khtml/id:kt008C7S3D/materials-selection-in/method-b-configuration.

[7] Ali Zubayar. *Mechanical Property Characterization of Polymeric Composites Mechanical Property Characterization of Polymeric Composites Reinforced by Continuous Microfibers Reinforced by Continuous Microfibers*. Tech. rep. South Dakota: Electronic Theses and Dissertations. 960, 2016. URL: https://openprairie.sdstate.edu/etd.

[8] P.K. Mallick. "Failure of polymer matrix composites (PMCs) in automotive and transportation applications". In: *Failure Mechanisms in Polymer Matrix Composites* (Jan. 2012), pp. 368–392. DOI: 10.1533/9780857095329.2.368.

[9] Mariam Al Ali AlMaadeed, Deepalekshmi Ponnamma, and Ali Alaa El-Samak. "Polymers to improve the world and lifestyle: physical, mechanical, and chemical needs". In: *Polymer Science and Innovative Applications: Materials, Techniques, and Future Developments* (Jan. 2020), pp. 1–19. DOI: 10.1016/B978-0-12-816808-0.00001-9.

[10] Mitsubishi Chemical Group. *Carbon Fiber FMC (CF-SMC)*.

[11] "Manufacturing of fibre–polymer composite materials". In: *Introduction to Aerospace Materials* (Jan. 2012), pp. 303–337. DOI: 10.1533/9780857095152.303.

[12] Matthew V. Rosato Dominick V. Rosato Donald V. Rosato. "Plastic Product Material and Process Selection Handbook". In: (2004), pp. 455–496.

[13] Jimmy Olsson. *Process Study on Compression Moulding of SMC using Factorial Design*. Tech. rep. Lueå: applied physics and mechanical engineering, 2008.

[14] P. Dumont et al. “Compression moulding of SMC: In situ experiments, modelling and simulation”. In: *Composites Part A: Applied Science and Manufacturing* 38.2 (2007), pp. 353–368. ISSN: 1359835X. DOI: 10.1016/j.compositesa.2006.03.010.

[15] M. L. Mehan and L. S. Schadler. “Micromechanical behavior of short-fiber polymer composites”. In: *Composites Science and Technology* 60.7 (May 2000), pp. 1013–1026. ISSN: 0266-3538. DOI: 10.1016/S0266-3538(99)00194-3.

[16] Dominick Rosato and Donald Rosato. “DESIGN PARAMETER”. In: *Plastics Engineered Product Design* (Jan. 2003), pp. 161–197. DOI: 10.1016/B978-185617416-9/50004-1.

[17] M. Piry and W. Michaeli. “Stiffness and failure analysis of SMC components considering the anisotropic material properties”. In: *Macromolecular Materials and Engineering* 284-285.1 (Dec. 2000), pp. 1–96. ISSN: 14387492. DOI: 10.1002/1439-2054(20001201)284:1<40::AID-MAME40>3.0.CO;2-3.

[18] Laurent Orgéas and Pierre J J Dumont. *SHEET MOLDING COMPOUNDS*. Tech. rep. Gernoble, France: Grenoble Institute of Technology, Feb. 2012.

[19] Paolo Feraboli et al. “Characterization of prepreg-based discontinuous carbon fiber/epoxy systems”. In: *Journal of Reinforced Plastics and Composites* 28.10 (May 2009), pp. 1191–1214. ISSN: 07316844. DOI: 10.1177/0731684408088883.

[20] S. FARA and A. PAVAN. “Fracture Mechanisms in Short Fibre Polymer Composites: The Influence of External Variables on Critical Fibre Angle”. In: *European Structural Integrity Society*. Vol. 32. C. Elsevier, Jan. 2003, pp. 387–398. DOI: 10.1016/S1566-1369(03)80111-5. URL: https://linkinghub.elsevier.com/retrieve/pii/S1566136903801115.

[21] S.S. Wang, H. Suemasu, and N.M. Zahlan. “Interlaminar Fracture of Random Short-Fiber SMC Composite”. In: *Sage Publications* 18.6 (Nov. 1984), pp. 574–594.

[22] Martin Tiefenthaler et al. “Characterization of the fracture mechanical behavior of C-SMC materials”. In: *16th Youth Symposium on Experimental Solid Mechanics, YSESM 2018*. Czech Technical University in Prague, 2018, pp. 1–5. ISBN: 9788001064740. DOI: 10.14311/APP.2018.18.0001.

[23] L. M. Martulli et al. “Weld lines in tow-based sheet moulding compounds tensile properties: Morphological detrimental factors”. In: *Composites Part A: Applied Science and Manufacturing* 139 (Dec. 2020). ISSN: 1359835X. DOI: 10.1016/j.compositesa.2020.106109.

[24] Luca Susmel et al. *Frattura ed Integrità Strutturale: Annals 2014: Fracture and Structural Integrity: Annals 2014*. Vol. 8. Gruppo Italiano Frattura, 2014, pp. 2–11.

[25] A. P. Chrysafi, N. Athanasopoulos, and N. J. Siakavellas. “Damage detection on composite materials with active thermography and digital image processing”. In: *International Journal of Thermal Sciences* 116 (June 2017), pp. 242–253. ISSN: 1290-0729. DOI: 10.1016/J.IJTHERMALSCI.2017.02.017.

[26] Carosena Meola, Giovanni Maria Carlomagno, and Luca Giorleo. “Geometrical limitations to detection of defects in composites by means of infrared thermography”. In: *Journal of Nondestructive Evaluation* 23.4 (Dec. 2004), pp. 125–132. ISSN: 01959298. DOI: 10.1007/s10921-004-0819-z.

[27] Liu Junyan, Liu Liqiang, and Wang Yang. “Experimental study on active infrared thermography as a NDI tool for carbon–carbon composites”. In: *Composites Part B: Engineering* 45.1 (Feb. 2013), pp. 138–147. ISSN: 1359-8368. DOI: 10.1016/J.COMPOSITESB.2012.09.006.

[28] Mahoor Mehdikhani et al. "Combining digital image correlation with X-ray computed tomography for characterization of fiber orientation in unidirectional composites". In: *Composites Part A: Applied Science and Manufacturing* 142 (Mar. 2021), p. 106234. ISSN: 1359-835X. DOI: 10.1016/J.COMPOSITESA.2020.106234.

[29] Hubert Schreier, Jean José Orteu, and Michael A. Sutton. *Image correlation for shape, motion and deformation measurements: Basic concepts, theory and applications*. Springer US, 2009, pp. 1–321. ISBN: 9780387787466. DOI: 10.1007/978-0-387-78747-3.

[30] Christopher M. Jackson et al. "Digital image correlation: Advancing mechanical property characterization of adhesive joints". In: *Advances in Structural Adhesive Bonding, Second Edition* (Jan. 2023), pp. 1035–1075. DOI: 10.1016/B978-0-323-91214-3.00014-4.

[31] GOM Zeiss company. *Digital Image Correlation and Strain Computation Basics*. Tech. rep. 2018.

[32] ASTM International. "D3171 - 22: Standard Test Methods for Constituent Content of Composite Materials". In: (2022). DOI: 10.1520/D3171-22. URL: www.astm.org..

[33] Michael T. Cann, Daniel O. Adams, and Claudio L. Schneider. "Characterization of fiber volume fraction gradients in composite laminates". In: *Journal of Composite Materials* 42.5 (Mar. 2008), pp. 447–466. ISSN: 00219983. DOI: 10.1177/0021998307086206.

[34] Instron. "Universal Testing Machine Compliance".

[35] Altair Optistruct. *Materials*. URL: https://2021.help.altair.com/2021/hwsolvers/os/topics/solvers/os/materials_os_r.htm.

[36] Altair Optistruct. *Altair Community - What is the difference between RBE-2 and RBE-3 elements?* URL: https://community.altair.com/community?id=community_question&sys_id=d9f99cb21be21954507ca6442a4bcbc1.

[37] Altair OptiStruct. *Contact*. URL: https://2021.help.altair.com/2021/hwsolvers/os/topics/solvers/os/contact_os_c.htm.

A

Appendix A

In Appendix A all objects including object 1, 2, 3, 4, 5, 6 and the stainless steel sample are presented in two views, one from an angle in order to get an overview of the sample's geometry and one side view of the objects. General measurements are shown in the figures.

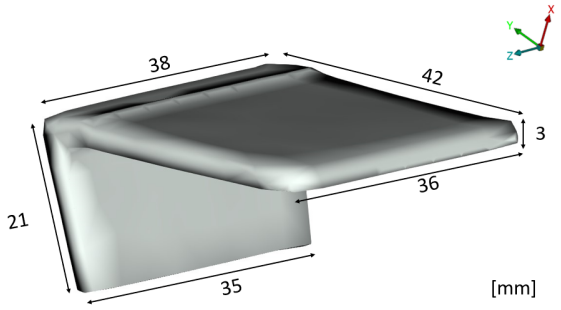

Figure A.1: Measurements of Object 1, on an angle.

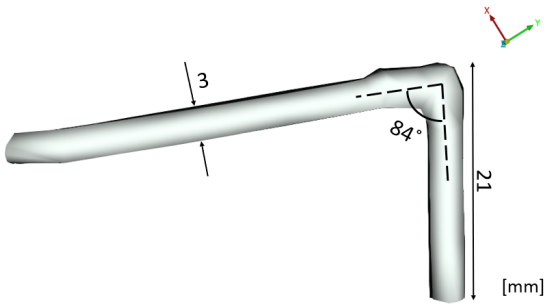

Figure A.2: Measurements of Object 1, from the side.

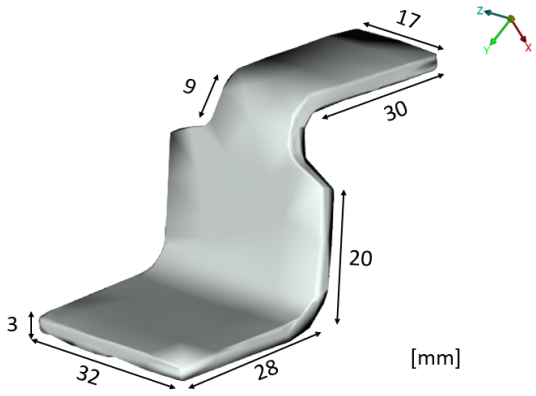

Figure A.3: Measurements of the first batch of Object 2, on an angle.

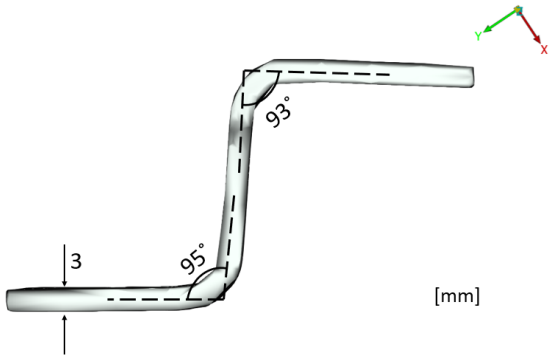

Figure A.4: Measurements of the first batch of Object 2, from the side.

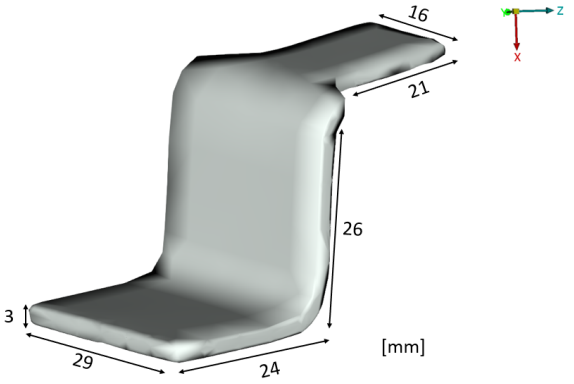

Figure A.5: Measurements of the second batch of Object 2, on an angle.

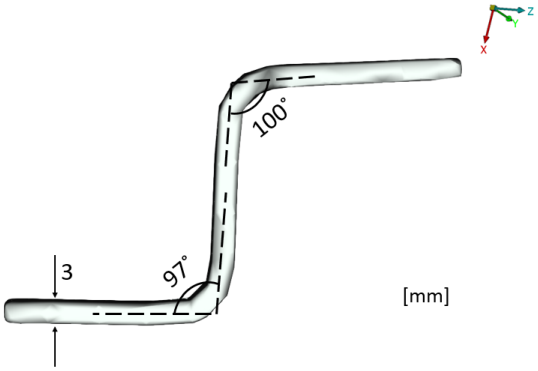

Figure A.6: Measurements of the second batch of Object 2, from the side.

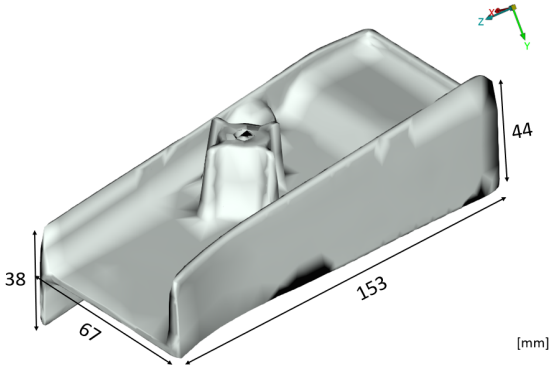

Figure A.7: Measurements of Object 3, on an angle.

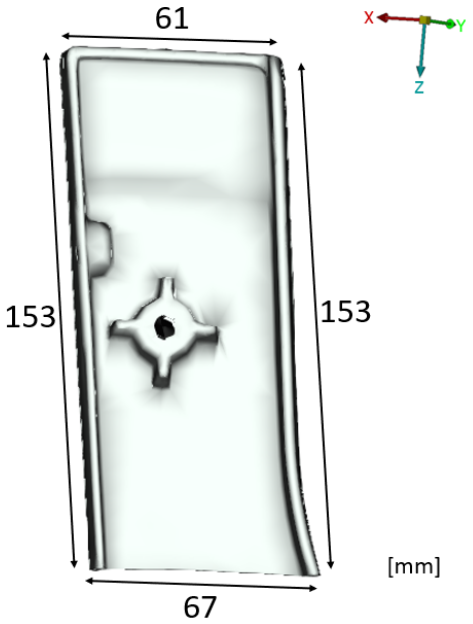

Figure A.8: Measurements of Object 3, from the top.

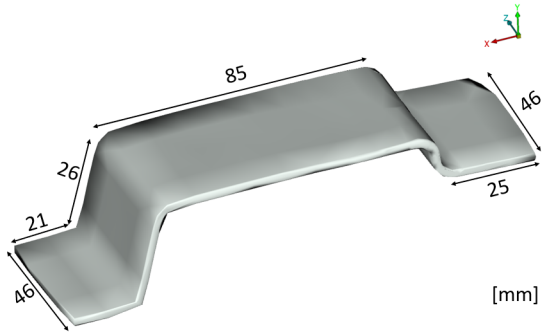

Figure A.9: Measurements of Object 4, on an angle.

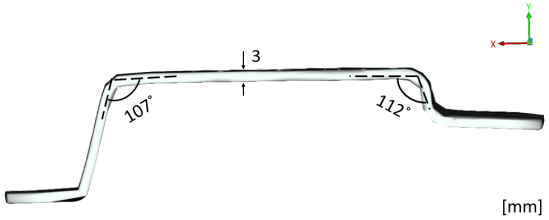

Figure A.10: Measurements of Object 4, from the side.

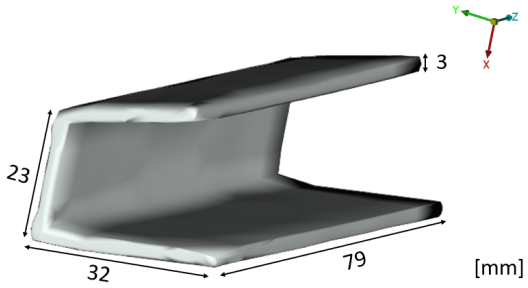

Figure A.11: Measurements of Object 5, on an angle.

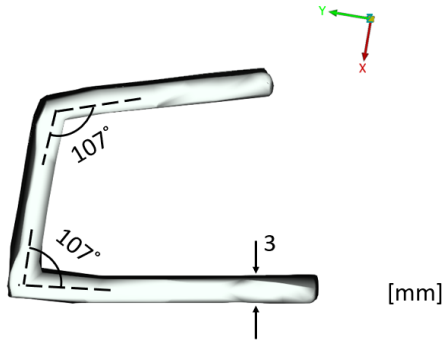

Figure A.12: Measurements of Object 5, from the side.

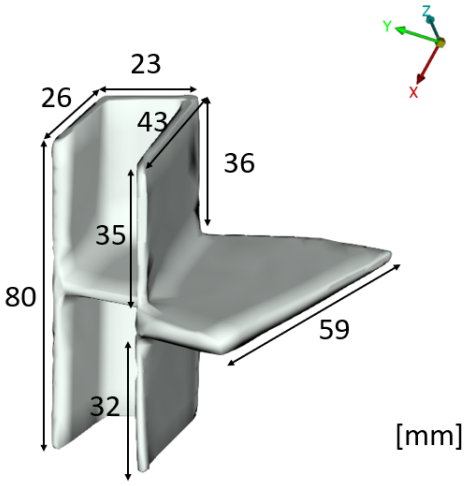

Figure A.13: Measurements of Object 6, on an angle.

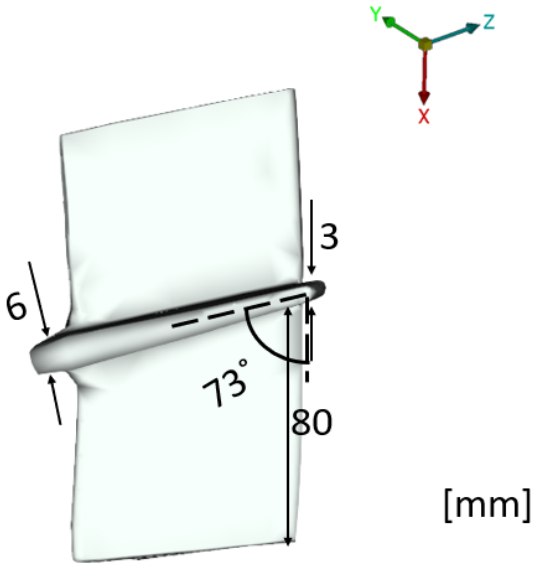

Figure A.14: Measurements of Object 6, from the side.

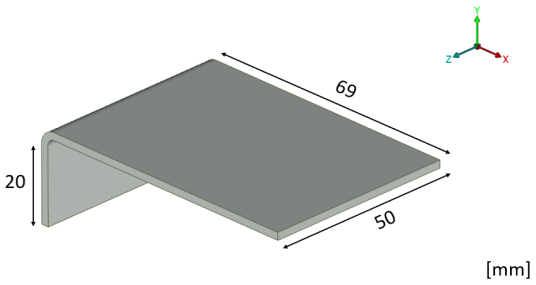

Figure A.15: Measurements of stainless steel sample, view from an angle.

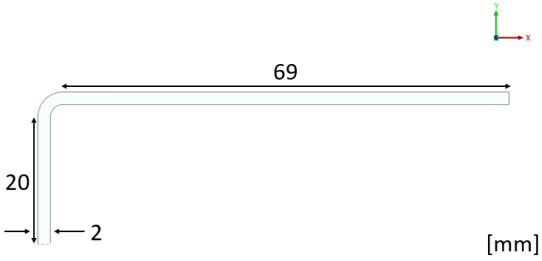

Figure A.16: Measurements of stainless steel sample, view from the side.

B

Appendix B

For object 5 problems were found with one of the samples which had a crack prior to testing. Sample B01_O05_S2 had a crack on an edge, close to the lower radius, prior to testing it. See Figure B.1 and Figure B.2. This has most likely appeared when cutting the sample.

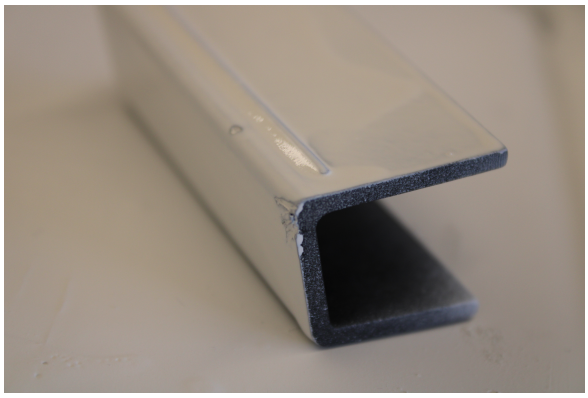

Figure B.1: B01_O05_S2's crack, can be seen in top radius.

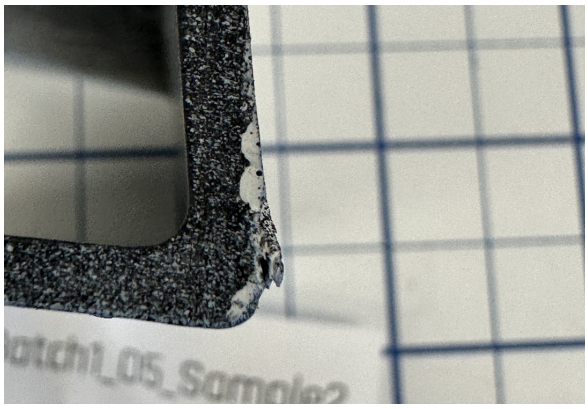

Figure B.2: B01_O05_S2's crack, can be seen the figure close to the edge.

Crack initiation position for the samples of object 5 can be seen below in Figure B.3 where batch 1 is presented and in Figure B.4 for batch 2. The crack initiations points are marked with a orange circle.

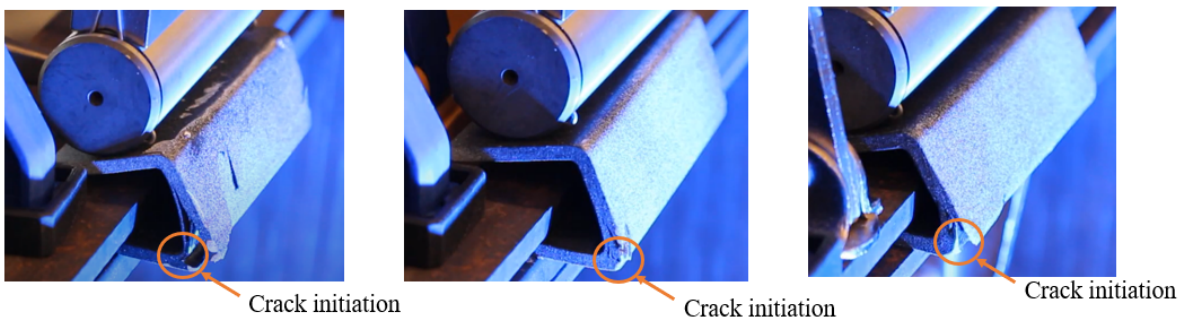

Figure B.3: Crack initiation points for object 5. To the left sample B01_O05_S1, in the middle B01_O05_S2 and to the right B01_O05_S3

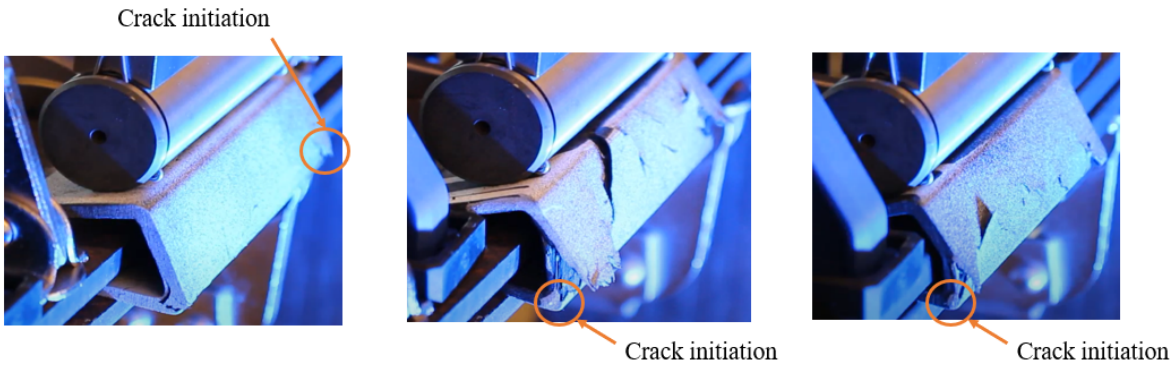

Figure B.4: Crack initiation points for object 5. To the left sample B02_O05_S1, in the middle B02_O05_S2 and to the right B02_O05_S3

C

Appendix C

In this appendix some pictures from the test setup is presented. It is presented regarding one tested object at the time.

Object 1

For object 1 The sample was clamped in two ways where the bold placement changed of the clamping steels. See Figure C.1 for the first clamping method and Figure C.2 for the second clamping method. Further, the solid aluminium load applicator can be seen in Figure C.3.

Figure C.1: The first clamping method, the bolts are places below the sample which induced a bending moment when testing.

Figure C.2: The second and used setup where the bolts where moved to the sides which clamped the sample better.

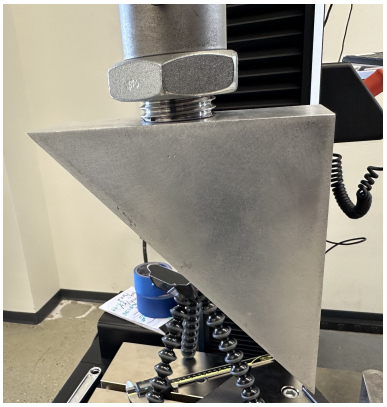

Figure C.3: Aluminium load applicator used for material test on Object 1 and stainless steel sample.

Object 2

The used tests setup for object 2 can be seen in Figure C.4.

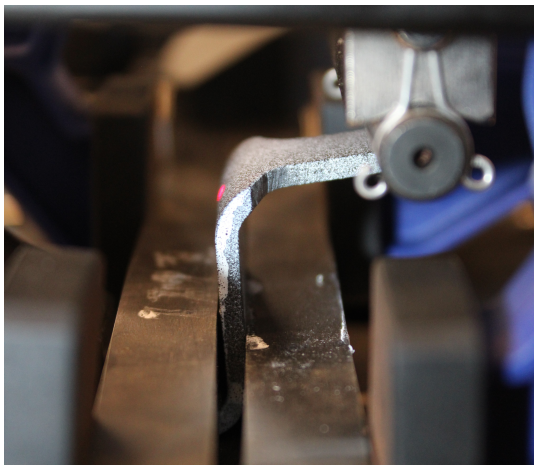

Figure C.4: Close picture of Object 2 test setup, the adjusted and second setup, where load applicator and clamping method are shown.

Object 4

The test setup for object 4 can be seen in the Figures C.5 and C.6 where a closer picture of the test setup where load applicators and clamping method can be seen as well as a more zoomed out figure where the GOM setup with cameras and light can be seen.

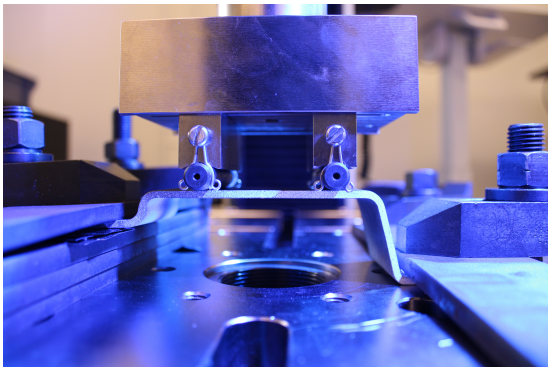

Figure C.5: A closer view of the test setup for object 4, load applicators and clamps can be seen.

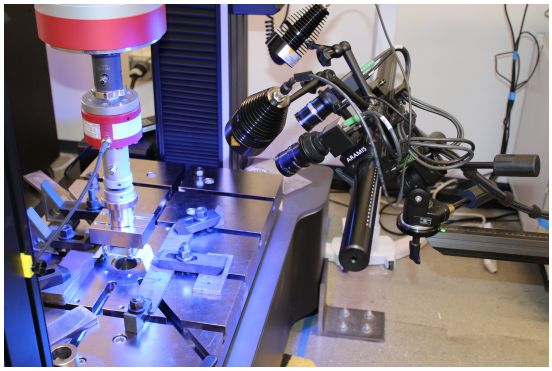

Figure C.6: The test setup for object 4, GOM system can be seen to the right in the figure.

Object 5

Two views of the test setup used for object 5 can be seen in Figure C.7 and Figure C.8

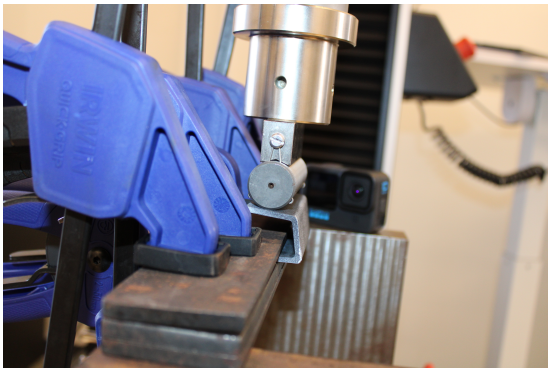

Figure C.7: A side view from the test setup of object 5.

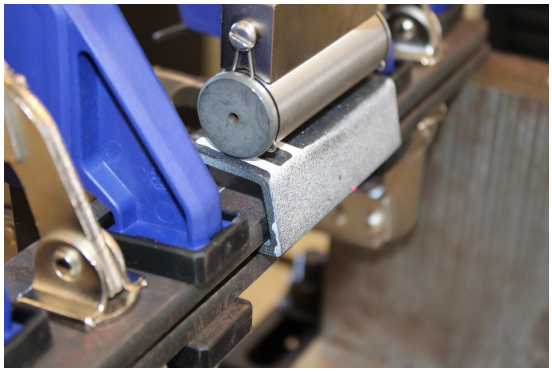

Figure C.8: Closer view of the test done on object 5.

Stainless Steel Sample

The two clamping methods used for the stainless steel sample can be seen on Figure C.9 and Figure C.10.

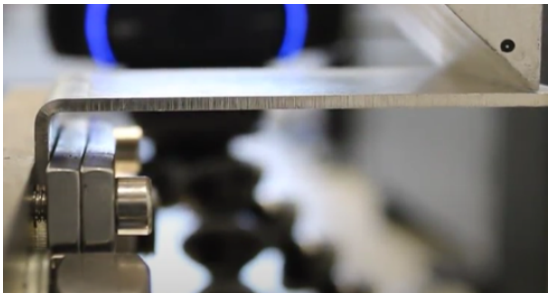

Figure C.9: Same clamping method as for object 1 which was custom made for the test.

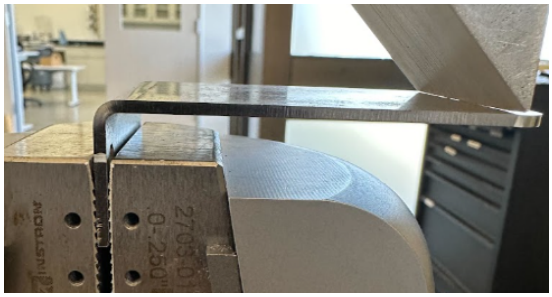

Figure C.10: A wise clamp used to validate the clamping method ised for object 1 and the steel sample.

D

Appendix D

Thermography scan results from the tested samples, except Object 5 due to having so many problems in the test an being ruled out for examination. In the following sections the results can be seen.

Object 1

For object 1 the markers for the points taken to plot the Time-Temperature graph. Point 1 (lower left) is red, point 2 (lower middle) is green, point 3 (lower right) is blue, point 4 (top left) is yellow, point 5 (top middle) is teal and point 6 (top right) is pink.

Figure D.1: Picture of B01_O01_S01 from thermography scan.

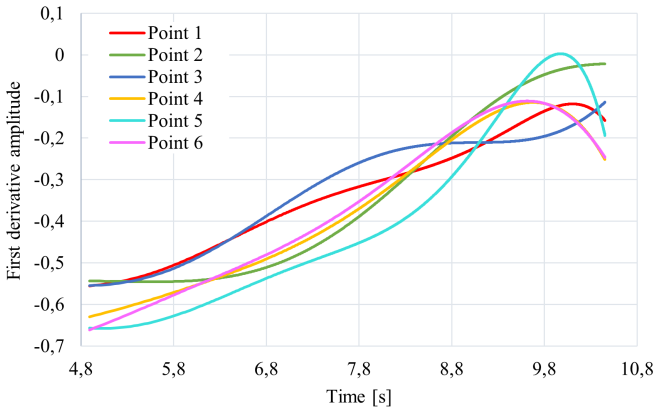

Figure D.2: Plot showing the Time-Temperature dependence of B01_O01_S01 where the time is the first derivative amplitude.

Object 2

For object 2 the markers for the points taken to plot the Time-Temperature graph. Point 1 (top left) is red, point 2 (top right) is green, point 3 (middle) is blue and point 4 (lower middle) is yellow. For batch 2 the yellow marker was not used.

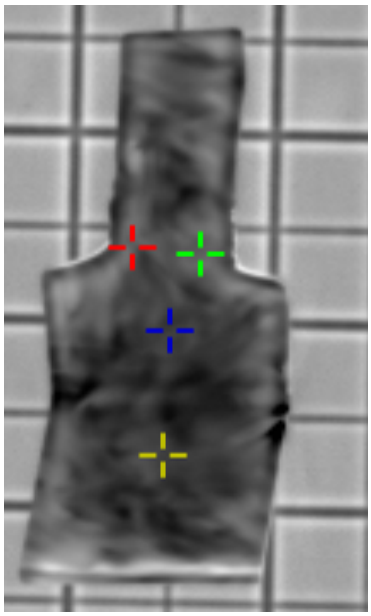

Figure D.3: Picture of B01_O02_S01 from thermography scan.

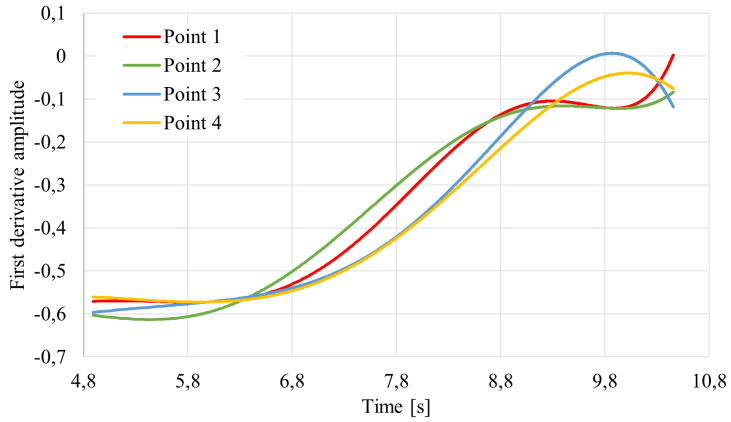

Figure D.4: Plot showing the Time-Temperature dependence of B01_O02_S01 where the time is the first derivative amplitude.

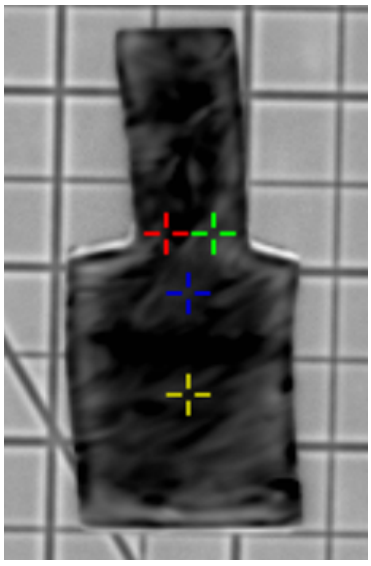

Figure D.5: Picture of B01_O02_S02 from thermography scan.

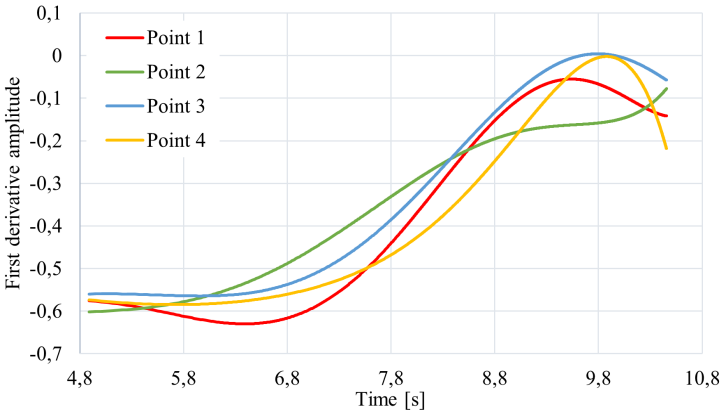

Figure D.6: Plot showing the Time-Temperature dependence of B01_O02_S02 where the time is the first derivative amplitude.

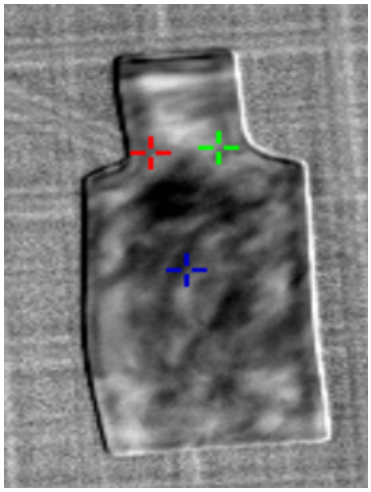

Figure D.7: Picture of B02_O02_S01 from thermography scan.

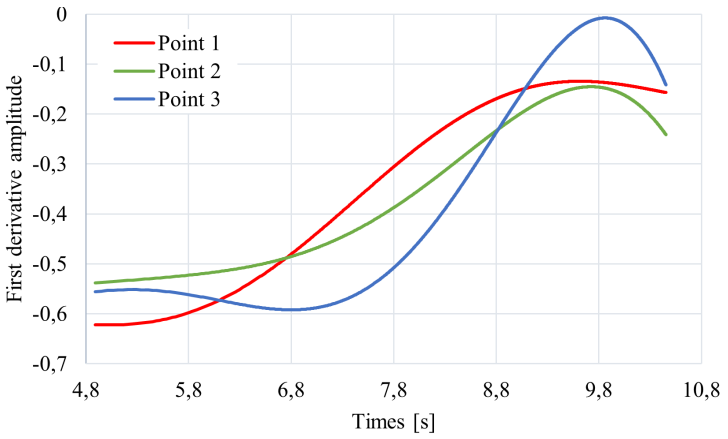

Figure D.8: Plot showing the Time-Temperature dependence of B02_O02_S01 where the time is the first derivative amplitude.

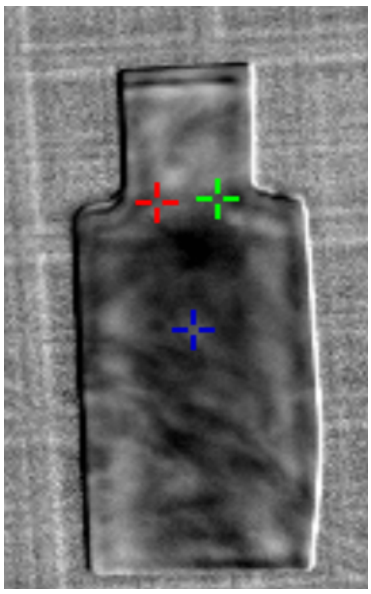

Figure D.9: Picture of B02_O02_S02 from thermography scan.

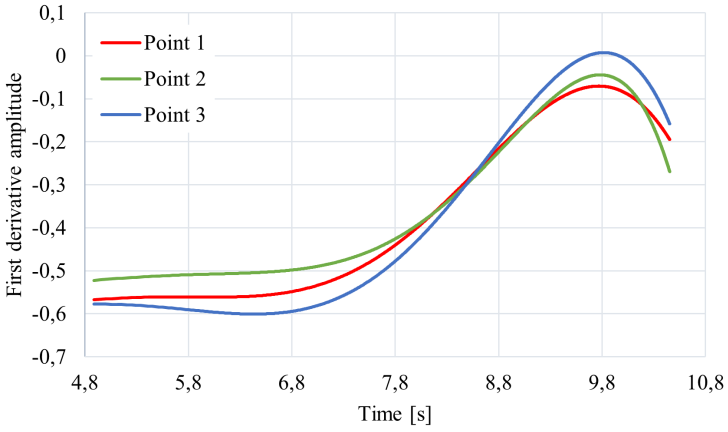

Figure D.10: Plot showing the Time-Temperature dependence of B02_O02_S02 where the time is the first derivative amplitude.

Object 4

Regarding object 4 the markers for the points taken to plot the Time-Temperature graph. Point 1 (top right) is red, point 2 (middle right) is green, point 3 (lower right) is blue, point 4 (top middle) is yellow, point 5 (middle middle) is teal, point 6 (lower middle) is pink, point 7 (top left) is orange, point 8 (middle left) is rose and point 9 (lower left) is brown.

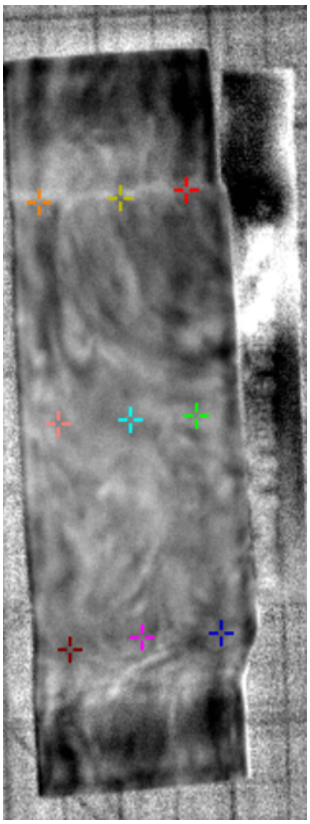

Figure D.11: Picture of B01_O04_S01 from thermography scan.

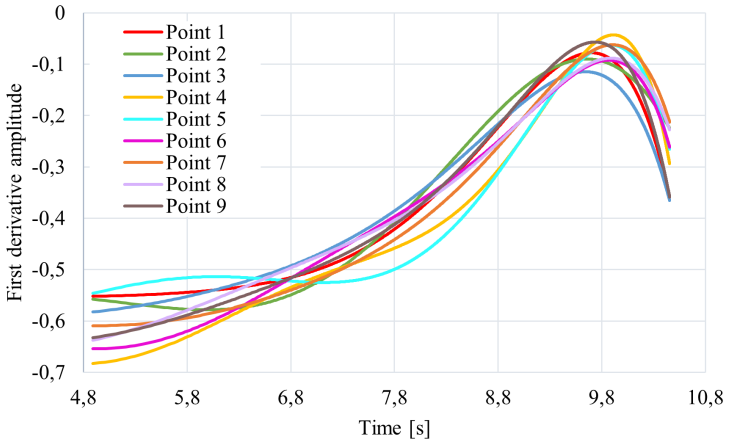

Figure D.12: Plot showing the Time-Temperature dependence of B01_O04_S01 where the time is the first derivative amplitude.

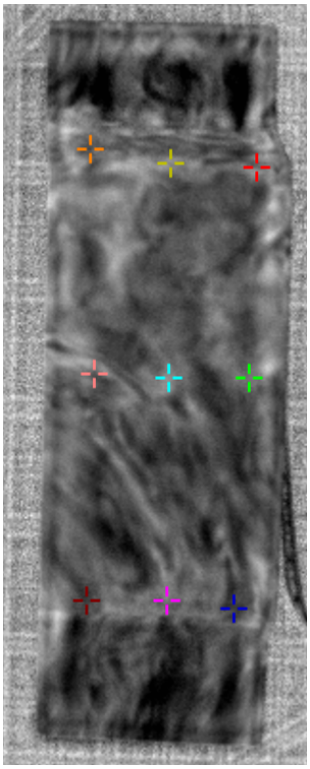

Figure D.13: Picture of B02_O04_S01 from thermography scan.

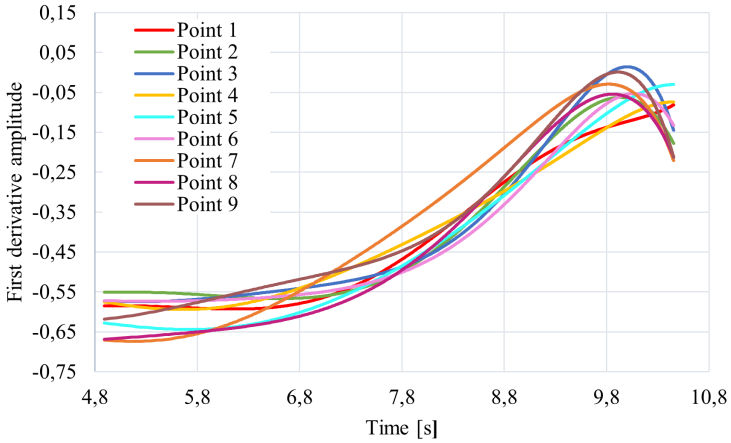

Figure D.14: Plot showing the Time-Temperature dependence of B02_O04_S01 where the time is the first derivative amplitude.

DEPARTMENT OF MECHANICS AND MARITIME SCIENCES
CHALMERS UNIVERSITY OF TECHNOLOGY
Gothenburg, Sweden 2024
www.chalmers.se

CHALMERS
UNIVERSITY OF TECHNOLOGY